HHS Public Access

Author manuscript

Nat Commun. Author manuscript; available in PMC 2015 May 10.

Published in final edited form as:

Nat Commun. ; 5: 5286. doi:10.1038/ncomms6286.

High-Resolution Structure and Mechanism of an F/V-Hybrid Rotor Ring in a Na^+-coupled ATP Synthase

Doreen Matthies[1,#], **Wenchang Zhou**[2,#], **Adriana L. Klyszejko**[1,§], **Claudio Anselmi**[2,§], **Özkan Yildiz**[1], **Karsten Brandt**[3], **Volker Müller**[3], **José D. Faraldo-Gómez**[2,4,*], and **Thomas Meier**[1,4,*]

[1]Department of Structural Biology, Max Planck Institute of Biophysics, Max-von-Laue-Strasse 3, 60438 Frankfurt am Main, Germany

[2]Theoretical Molecular Biophysics Section, National Heart, Lung & Blood Institute, National Institutes of Health, Bethesda, MD 20892, USA

[3]Molecular Microbiology & Bioenergetics, Institute of Molecular Biosciences, Goethe University of Frankfurt, Max-von-Laue-Strasse 9, 60438 Frankfurt am Main, Germany

[4]Cluster of Excellence Macromolecular Complexes, Goethe-University, Max-von-Laue-Strasse 15, 60438 Frankfurt am Main, Germany

Abstract

All rotary ATPases catalyze the interconversion of ATP and ADP-P_i through a mechanism that is coupled to the transmembrane flow of H^+ or Na^+. Physiologically, however, F/A-type enzymes specialize in ATP synthesis driven by downhill ion diffusion, while eukaryotic V-type ATPases function as ion pumps. To begin to rationalize the molecular basis for this functional differentiation, we solved the crystal structure of the Na^+-driven membrane rotor of the *Acetobacterium woodii* ATP synthase, at 2.1 Å resolution. Unlike known structures, this rotor ring is a 9:1 heteromer of F- and V-type c-subunits, and therefore features a hybrid configuration of ion-binding sites along its circumference. Molecular and kinetic simulations are used to dissect the mechanisms of Na^+ recognition and rotation of this c-ring, and to explain the functional implications of the V-type c-subunit. These structural and mechanistic insights indicate an evolutionary path between synthases and pumps involving adaptations in the rotor ring.

[*]*Corresponding authors:* TM: thomas.meier@biophys.mpg.de, J.D.F–G: jose.faraldo@nih.gov.
[#]These authors contributed equally
[§]These authors contributed equally

Author Contributions

T.M. and V.M. conceived experiments; J.D.F-G and C.A. conceived computations; D.M. purified and crystallized the protein. D.M., T.M. and O.Y. collected data; D.M. and O.Y. solved the structure; A.L.K. obtained and analyzed AFM images; K.B. provided cell membranes; D.M., A.L.K. and T.M. interpreted experimental data; W.Z. and C.A. performed and analyzed computations; W.Z., C.A. and J.D.F.-G. interpreted computational results; J.D.F-G, D.M., T.M., W.Z., C.A and A.L.K. wrote the paper. This work is dedicated to Michael Fritz († 2012), who worked on 2D and 3D crystallization experiments of the *A. woodii* c-ring in the laboratories of V.M. and T.M.

Accession Codes

Coordinates and structure factors have been deposited at the Protein Data Bank with the accession code 4BEM.

Competing Financial Interests Statement

The authors declare no competing financial interests.

Introduction

Rotary ATPases are ubiquitous membrane-bound macromolecular enzymes with similar architecture and mechanism but two distinct physiological functions. All rotary ATPases consist of a transmembrane domain, which mediates the permeation of H^+ or Na^+, and a soluble domain, where ATP is either hydrolyzed or synthesized[1] (Supplementary Fig. 1). Catalysis in the soluble domain is coupled to the rotation of a sub-complex within the membrane domain, known as the c-ring, against a static, adjacent element, known as subunit-a. Viewed from the soluble domain, this rotation is clockwise when the enzyme hydrolyzes ATP, leading to active ion transport. If the mechanism is instead driven by ion flow down the gradient, the c-ring rotates counter-clockwise and ATP is synthesized. Although the directionality of this rotary mechanism can be typically reversed *in vitro*[2–5], individual enzymes are functionally specialized *in vivo*. F-type enzymes, in the membranes of bacteria, mitochondria and chloroplasts, function as ATP synthases[6]. A-type enzymes are also synthases, but are specific to archaea[7]. V-type enzymes, however, function as ATP-driven ion pumps in eukaryotic vacuolar membranes[8].

This physiological specialization suggests that structural adaptations might have evolved to optimize a given functionality. A long-standing hypothesis is that the c-subunits that constitute the rotor ring might contribute to this differentiation[9]. Prototypical c-rings of bacterial and eukaryotic ATP synthases are homomers of c-subunits with a simple topology, namely a hairpin of two transmembrane helices[10–14] (Supplementary Fig. 2). The number of c-subunits assembled varies across species (from 8 to 15 to date[15,16]), but canonical F-type c-rings consistently feature an uninterrupted series of ion-binding sites along their outer circumference, each located at the interface between two adjacent hairpins, approximately halfway across the membrane. The prototypical c-rings of ATP-driven pumps, however, typically consist of c-subunits with double hairpins[17], presumably resulting from gene duplications[18]. Intriguingly, these rings usually feature fewer ion-binding sites due to mutation of key amino-acids required for ion coordination (Supplementary Fig. 2). Moreover, some eukaryotic V-type c-rings seem to consist of c-subunits with different amino-acid sequence. For example, the c-ring of the vacuolar ATPase of *Saccharomyces cerevisiae* appears to be a heteromer of three different double-hairpin c-subunits (c, c′, c″), though its stoichiometry remains unclear[19–21].

To begin to rationalize how the evolution of the c-ring may have contributed to the functional specialization of different rotary ATPase subfamilies, we isolated the c-ring from the F-type ATP synthase of *Acetobacterium woodii*, and solved its structure by X-ray crystallography. Consistent with previous biochemical studies[22] we find that this c-ring consists of a combination of prototypical F- and V-type c-subunits, thus resembling an evolutionary intermediate. The structure provides the basis for molecular and kinetic simulations, through which we examine the mechanistic and thermodynamic implications of this unprecedented hybrid stoichiometry.

Results

Structure of the *Acetobacterium woodii* c-ring

The crystal structure of the c-ring from the *A. woodii* ATP synthase was resolved at 2.1 Å resolution (Supplementary Fig. 3; Supplementary Table 1). Consistent with our previous biochemical analysis[22], the ring is an assembly of nine copies of single-hairpin c-subunits, referred to as $c_{2/3}$, and one copy of a double-hairpin c-subunit, or c_1 (Fig. 1a,b). Thus, the structure consists of 22 transmembrane α-helices, arranged in two concentric, staggered rings of eleven helices each. The c-ring is ~72 Å in height, and is shaped like an hourglass with a central pore perpendicular to the membrane plane (Fig. 1). The outermost diameter is widest (~55 Å) on the cytoplasmic and periplasmic sides, and is narrowest approximately halfway across the membrane (~45 Å). In the $c_{2/3}$ subunits, the N-terminal (or inner) helix and the C-terminal (or outer) helix are connected on the cytoplasmic side by a short, rigid loop, which mediates crystal contacts (Supplementary Fig. 4). The $c_{2/3}$ subunits are structurally very similar (RMSD < 1 Å) to other F-type single-hairpin c-subunits (Supplementary Fig. 5), particularly those in the *Ilyobacter tartaricus* c_{11} ring[12] (RMSD ~ 0.4 Å).

The c_1 subunit consists of 4 transmembrane helices, and thus resembles a prototypical V-type c-subunit. The first and third helices are part of the inner ring while the second and fourth face the lipid bilayer (Fig. 1a,b). An unusual α-helical extension at the N-terminus of the c_1 subunit is also well resolved, projecting across the central pore towards a distal $c_{2/3}$ subunit, parallel to the membrane plane. The loop that connects the two hairpins in c_1 on the periplasmic side, which is significantly longer than the cytoplasmic loops within each of the hairpins, can be clearly discerned too. Aside from these two features, the structure of c_1 is nearly identical to that of two adjacent $c_{2/3}$ subunits (RMSD ~ 0.3 Å) (Supplementary Fig. 5), and is also similar to the double-hairpin c-subunit of the V-type ATPase from *Enterococcus hirae*[17] (RMSD < 2 Å).

The membrane-exposed face of the c-ring is primarily hydrophobic (Fig. 1c); neighboring electron densities likely correspond to bound detergent molecules, marking the boundaries of the lipid bilayer (~30 Å) (Fig. 1c). The surface of the central pore is also highly hydrophobic (Fig. 1d), and residual electron densities visible therein seem to also originate from disordered detergent molecules. The pore diameter is ~17 Å at its narrowest, and the length of the hydrophobic region is ~30 Å. Thus, in native membranes this pore is probably occluded by a lipid bilayer formed by a handful of molecules, slightly shifted towards the periplasm.

The periplasmic and cytoplasmic sides of the c-ring are rich in charged and polar amino acids (Fig. 1e,f). The cytoplasmic surface is largely electronegative, due to a glutamate residue in the cytoplasmic loop of the $c_{2/3}$ subunits (sequence RQPE) (Fig. 1e,f; Supplementary Fig. 2). Interestingly, the two hairpin loops in the c_1 subunit (of sequence KNPT and IRPE, respectively) alter this pattern, and the surface here is electropositive, which may enhance the interaction of the c-ring with subunits γ and ε. In F-type ATP synthases, these subunits form a sub-complex referred to as the central stalk, which is essential to mechanically couple the ion-conducting and catalytic domains. On the

periplasmic side, the N-terminal helix in the c_1 subunit occludes the central pore almost completely (Fig. 1f). Nevertheless, small openings between this helix and the inner pore wall remain, which could conceivably allow passage of protons, ions or water. It is thus likely that the pore is actually sealed by lipid molecules, as observed in other rings[23–25], so as to prevent the dissipation of the electrochemical gradient across the membrane.

The Na^+-binding sites in the *A. woodii* c-ring

The *A. woodii* c-ring features a series of Na^+-binding sites on its lipid-exposed outer surface, close to the membrane center (Fig. 1a,b). Specifically, binding sites occupied by Na^+ can be clearly discerned at each of the eight interfaces between single-hairpin $c_{2/3}$ subunits, sandwiched between the two outer helices, as well as at the two interfaces between $c_{2/3}$ and c_1 subunits (Fig. 2a,b,d). Na^+ is electrostatically stabilized by a glutamate side-chain, located in the outer helix of one of the flanking c-subunits. A carboxylate group at this position is conserved in all known c-ring binding sites, both in enzymes coupled to Na^+ [12,17,26] as well as those coupled to H^+, which bind to the c-ring by protonation[13,27,28,14]. Three other protein groups coordinate the ion: a glutamine carbonyl, from the inner helix of the same subunit as the key glutamate; and a threonine hydroxyl and a backbone carbonyl, from the outer helix of the adjacent subunit (Fig. 2; Supplementary Table 2). Consistent with other structures of Na^+-coupled c-rings[29,26], a bound water molecule co-coordinates Na^+ in all sites (Fig. 2; Supplementary Table 2). This ion-coordination network is stabilized by several peripheral side-chains, e.g. hydrogen-bonds can be inferred between the key glutamate and a tyrosine, and between the bound water molecule and a threonine (Fig. 2a,b,d). Although this motif is chemically selective for protons[30,31], the much larger amount of sodium ions over protons in the crystallization buffer (100 mM Na^+ and pH 4.5) ensures Na^+ binding. This concentration effect is also present physiologically, and hence this crystal structure confirms earlier functional measurements indicating that ATP synthesis in *A. woodii* is driven directly by a sodium-motive-force[32].

Interestingly, the potential binding site at the interface between the two hairpins within the c_1 subunit lacks a Na^+ ion (Fig. 2c,e,f; Supplementary Fig. 6). This site is rich in polar groups, and a water molecule can be clearly discerned in the electron density map, forming hydrogen bonds with the protein and with each other (Fig. 2c,f). However, no density for Na^+ was detected, despite the high Na^+ concentration in the crystallization buffer. This is due to the substitution of the prototypical carboxyl side-chain by glutamine (Gln162); because of its neutral charge, the carboxamide group cannot offset the cost of Na^+ dehydration upon binding to a site immersed in a mostly hydrophobic environment (i.e. detergent in the crystal). We conclude, therefore, that in a complete revolution the *A. woodii* c-ring transports 10 ions across the membrane.

Direct visualization of the c-ring by AFM

The N-terminal α-helical extension of the c_1 subunit is ~20 amino acids in length and partially hydrophobic. In the crystal structure this helix lies across the central pore, rather than being inserted in the membrane (Fig. 1b). To assess whether this is the native conformation, we studied a series of 2-dimensional arrays of *A. woodii* c-rings via atomic

force microscopy (AFM), in a physiological buffer and at room temperature (Fig. 3a). We specifically analyzed the periplasmic face of the c-ring via single-particle classification and averaging (Methods). The five class-averages obtained consistently show 10 identical density peaks along the c-ring circumference, followed by a depression (Fig. 3b,c; Supplementary Fig. 7). Adjacent to it, in the clock-wise direction, a rod-like density projects across the central pore of the ring, in an orientation that is similar in all class averages. This rod is the highest object in the density, particularly in close proximity to its distal end (Fig. 3d,e). All these features are consistent with the crystal structure: the regular pattern of densities along the ring circumference corresponds to the elongated N-termini of the $c_{2/3}$ subunits, which protrude from the membrane; the depression in this pattern is the loop connecting the two c_1 subunit hairpins, which protrudes less than the $c_{2/3}$ N-termini; and lastly, the rod projecting across the pore is the N-terminal extension of the c_1 subunit. Thus, the AFM data confirms both the $9c_{2/3}$:$1c_1$ stoichiometry of the *A. woodii* c-ring and the conformation of the c_1 N-terminal α-helix observed in the crystal structure.

The role of this α-helical extension is, however, not apparent. Given its conformation, it is unlikely to be directly involved in the mechanism of the enzyme. A reasonable speculation is that it contributes to make c-rings with a $9c_{2/3}$:$1c_1$ stoichiometry more statistically abundant than those with a greater number of c_1 subunits. In previous studies of the factors controlling c-ring assembly, we have shown that several stoichiometries co-exist in equilibrium, albeit one form is thermodynamically dominant, particularly for native amino-acid sequences[5,33]. Since the observed conformation of this amphipathic helix is sterically possible only if the ring contains one c_1 subunit, other oligomeric states (for example $7c_{2/3}$:$2c_1$) would necessarily expose a large hydrophobic surface to water, and hence be energetically disfavored.

Mechanism of Na^+ loading and release

The ion-locked conformation of the Na^+-binding sites in the structure of the *A. woodii* c-ring (Fig. 2) is very similar to that observed in other high-resolution c-ring structures resolved using detergent-based crystallization buffers[12,17,13,28,26]. We have previously shown, for a H^+-coupled c-ring, that this is the configuration of the sites that face the membrane during the enzyme's rotary cycle[34]. The pK_a of these sites is highly elevated thus they do not exchange protons with the bulk solution. Proton loading and release, either downhill or uphill, takes place instead when the sites become sequentially exposed to the adjacent subunit-a as the c-ring rotates around its axis[35,36]. The atomic structure of subunit-a is to date unknown, but cysteine-accessibility measurements have indicated that this subunit and/or its interface with the c-ring feature two aqueous channels that reach the c-ring ion-binding sites from either side of the membrane[37]. Our previous analysis showed that this hydrated micro-environment facilitates proton exchange by triggering a local conformational change in the binding sites, and by shifting down their pK_a[34]. Specifically, hydration causes the key glutamate side-chain to adopt an exposed outward orientation that facilitates reversible deprotonation, without the need of a competing electrostatic interaction. This proposal was recently validated by high-resolution structures of a mitochondrial H^+-coupled c-ring, solved using a detergent-free crystallization buffer primarily consisting of 2-methyl-2,4-pentanediol (MPD) in water[14]. This amphiphilic compound coats the

hydrophobic surface of the c-ring, but unlike detergent, it permits the H^+-binding sites to be hydrated[14]. Accordingly, the binding sites in the mitochondrial c-ring structure adopt the predicted unlocked conformation[34], and can become deprotonated[14].

To assess whether this mechanism applies to the *A. woodii* ATP synthase and other Na^+-coupled ATPases, we carried out a series of molecular dynamics simulations of the *A. woodii* c-ring solubilized in an MPD/water buffer (Supplementary Fig. 8; Supplementary Fig. 9). Spontaneous Na^+ dissociation events were indeed observed in independent simulations, after 100–200 ns (Fig. 4a). The mechanism of Na^+ unloading is very similar to that proposed previously for H^+ (Fig. 4b; Supplementary Movie 1). The Na^+ ion exits the binding site along with the key glutamate, as this side-chain rotates outwards in what appears to be a thermal fluctuation. As water molecules gradually penetrate the binding site, disrupting the network of hydrogen-bonding interactions therein, Na^+ remains transiently bound to the carboxyl group, but upon formation of a complete water-coordination shell, the ion diffuses away, while the glutamate side-chain continues to project towards the solvent.

To investigate the process of ion loading, a third simulation was initiated about 50 ns after a Na^+ unbinding event. After another ~100 ns, we observed spontaneous, uncorrelated rebinding of the ion, via a mechanism that is analogous to that of the unbinding events, but in reverse (Fig. 4; Supplementary Movie 2; Supplementary Fig. 10). That is, the key glutamate recognizes the ion, whose water-coordination sphere becomes depleted. Next the carboxyl-ion pair enters the binding site expelling most of the water therein. In the final bound state, only the water molecule that co-coordinates the ion in the experimental crystal structure remains in the site, exactly in the same location.

In summary, these simulations show that Na^+ loading and release from the c-ring entails localized conformational changes in the binding sites. As we showed previously for protons[34], Na^+ release is facilitated by hydration, and does not require a competing ionic interaction, e.g. between the key glutamate and subunit-a. Likewise, empty binding sites do not require a stabilizing ionic interaction to remain in a configuration suitable for Na^+ recognition; local hydration is sufficient. It should be noted that comparable simulations of the *A. woodii* c-ring in a phospholipid membrane revealed no dissociation events (Fig. 4a; Supplementary Fig. 8).

Dynamics of the c_1 site in response to hydration

The simulations just described also provide insights into the dynamics of the site within the c_1 subunit that lacks a bound Na^+. In the crystal structure, this site adopts a conformation akin to that observed in the proton-binding sites of several H^+-dependent c-rings[13,38,28]. Specifically, the glutamine (Gln162) that replaces the prototypical glutamate is locked in position by several hydrogen-bonds with neighboring side-chains (Gln129 and Thr80), as well as with a bound water molecule. In simulations of the c-ring in a phospholipid bilayer, this locked configuration was indeed the most frequently observed (Fig. 5a,c). In the MPD/water buffer, however, the locked conformation is in equilibrium with a range of configurations in which the H-bonding network in the site is disrupted by water molecules, and Gln162 projects out into the solvent (Fig. 5b,c). These results indicate that, upon entering the subunit-a interface, the dynamic response of the c_1 site resembles that of the

ion-binding sites in this and other c-rings[34]. It is worth noting, though, that the c_1 site does not bind Na^+ even in this hydrated environment. Additional simulations in which a Na^+ ion is carefully modeled into the c_1 site (Methods; Fig. 5d) consistently show immediate dissociation, in the ~10 ns time-scale (Fig. 5e). This dissociation rate is much faster than what we observe for the actual Na^+-binding sites, i.e. microsecond time-scale or longer (note Fig. 4a shows single dissociation events out of ten possible), indicating the Na^+ affinity of the c_1 site is several orders of magnitude weaker.

Directionality and mechanism of c-ring rotation

The directionality of the rotary mechanism of ATPases can be fully rationalized using the two-channel model mentioned earlier[35,36]. This model postulates (i) that the aqueous pathways across the a/c complex are two discontinuous half-channels, each open to one side of the membrane and (ii) that these channels reach to two adjacent binding sites in the c-ring, such that the site exposed to the N-side of the membrane (i.e. with negative electrochemical potential), which we refer to as S_N, is located clockwise (as viewed from F_1) relative to the site exposed to the P-side (i.e. with positive electrochemical potential), or S_P. An additional and crucial assumption is that ions must not be able to transfer directly from S_P to S_N, or vice versa. Instead, an ion that binds, for example, to S_P, would reach S_N only when the c-ring makes a near-complete revolution, counter-clockwise.

A conserved arginine residue in subunit-a, proximal to the c-ring ion-binding sites[39], is thought to interact with the conserved glutamate/aspartate in the c-subunits and to be an important element in this mechanism[40,41]. Although it is often imagined that this interaction is a necessary trigger for ion release from the c-ring, the calculations presented above and elsewhere[34,14] indicate that this is not so; a hydrated microenvironment is in fact sufficient to induce the release of ions from the c-ring. Consistent with this notion, functional assays of the *E. coli* ATP synthase have demonstrated that neutralizing mutations of the subunit-a arginine do not preclude downhill ion diffusion across the a/c complex; the mutations, however, abolish the coupling between ion permeation and catalysis, i.e. impair the rotary mechanism of the enzyme[41,42]. What then is the role of the conserved arginine in subunit-a?

In our version of the two-channel model, depicted in Fig. 6, the role of this side-chain is to sequester one of the two binding sites at the a/c interface, already in the ion-free state, so as to preclude direct ion hopping between them. Thus, an ion that binds to S_P from the P-side, while S_N is engaged by the arginine, would not be able to hop directly to S_N and thus leak through the N-channel; conversely, an ion that exits S_N, while S_P is engaged, would be necessarily released on the N-side of the membrane, and not via the P-channel.

To evaluate this key element of the mechanism, we calculated the free-energy cost associated with the transfer of a Na^+ ion from a loaded binding site in the *A. woodii* c-ring (i.e. S_P) to an adjacent empty site, clockwise (i.e. S_N), in which the exposed carboxyl group is paired with a guanidinium ion (GND^+), modeled in so as to mimic the interaction with the conserved arginine on subunit-a (Fig. 7a,b). The resulting free-energy value was ~9 kcal/mol (Fig. 7c). That is, an ion reaching S_P through the P-channel would be more than a million times more likely to remain in S_P than to hop to S_N. Ion hopping would be also far less probable than the alternative next step in the proposed cycle, namely the rotational

displacement of the c-ring (Fig. 6). The energy cost of this rotational displacement is about ~3 kcal/mol, i.e. three times the free energy cost of ATP synthesis at typical ATP/ADP/P_i concentrations (~11 kcal/mol), distributed over eleven steps. Direct ion hopping between the two c-ring binding sites exposed at the a/c interface is therefore extremely improbable, even from a purely thermodynamic standpoint (i.e. even if we neglect kinetic barriers). This electrostatic separation between the P- and N-channel ensures strict coupling between ion permeation and c-ring rotation.

Energetics of the arginine-switch step

A necessary step in the microscopic mechanism proposed in Fig. 6 requires the key arginine side-chain in subunit-a to switch between two competing interactions with the glutamate side-chains in the c-ring that are exposed to the a/c interface, S_P and S_N. Whether or not this hypothetical step is plausible, from an energetic standpoint, remains to be qualified. For the *A. woodii* ring in particular, it is unclear whether the glutamine side-chain in the V-type c_1 subunit is a viable interaction partner. To address these questions, we first designed a free-energy calculation in which a GND^+ ion reversibly exchanges between two adjacent Na^+ sites in empty $c_{2/3}$ subunits, i.e. the glutamate side-chains in these sites project out into the MPD/water buffer, and form competing ion-pairs with GND^+ in the course of the simulation. These two states are not structurally symmetric, but nevertheless our calculations show they are equivalent energetically (Fig. 8a). More surprisingly, the calculations reveal that the energy barrier between them is only ~4 kcal/mol (comparable to e.g. the isomerization of a single carbon-carbon bond in a linear alkane chain). Analysis of the simulated exchanges reveals this energetic penalty is small because in the transition state the GND^+ ion remains indirectly engaged to both carboxylate groups via ordered layers of water molecules (Fig. 8a; Supplementary Fig. 11a). Thus, hydration at the a/c interface not only facilitates ion release from the c-ring binding sites, but also eases the exchange between consecutive c-subunit/subunit-a interactions.

We next carried out two analogous free-energy simulations in which the GND^+ ion exchanges between an unlocked glutamate in a $c_{2/3}$ subunit and the glutamine in the c_1 subunit, either in the clockwise (Fig. 8b; Supplementary Fig. 11b) or counter-clockwise directions (Fig. 8c; Supplementary Fig. 11c). Both calculations showed transient binding of GND^+ to the c_1 glutamine via its carboxamide group. Not surprisingly, the Gln-GND^+ pair is energetically less favorable than Glu-GND^+, but the computed free-energy difference is only ~4 kcal/mol (while the barrier between the two states is about 5 kcal/mol). To put this energetic cost in context, note that the necessary release of a bound Na^+ from the S_N site (Fig. 6) entails a free-energy expenditure of ~3 kcal/mol (for K_D ~ 0.1 mM and $[Na^+]_N$ ~ 10 mM). Thus, while the formation of the Gln-GND^+ interaction is likely to slow down the rotary mechanism (see below), this step is not prohibitive from an energetic standpoint. Indeed, a statistical analysis of arginine interactions with ionic and non-ionic side-chains in experimental high-resolution protein structures underscores the feasibility of this kind of interaction (Supplementary Fig. 12).

Thus, we conclude that the proposed arginine-switch step (Fig. 6) is plausible from an energetic standpoint, both in prototypical F-type rings as well as in *A. woodii*. Nevertheless,

our results indicate that the glutamate-to-glutamine substitution in the V-type c_1 subunit not only precludes Na^+ binding, but also introduces a non-negligible energetic cost in the dynamic exchange between c-ring/subunit-a interactions. Its impact on the kinetics of c-ring rotation and on the transduction of the sodium-motive-force are analyzed next.

Thermodynamic and kinetic impact of the V-type c-subunit

The rotary mechanism of F-, A- and V-type ATPases is a natural consequence of the inherent periodicity of the conformational free-energy landscape of the subunit-a/c-ring complex. Due to the oligomeric architecture of the c-ring, this landscape consists of a series of resting states, which may interconvert in either direction, stepwise, as ions bind to and become released from the c-ring. The detailed features of this landscape surely vary among different enzymes, but a general implication of the two-channel model described above is that counter-clockwise steps result in ion permeation from the P to the N-side, and *vice versa* for clockwise steps. Moreover, when the a/c complex is isolated from the catalytic domain the preferred directionality of these individual steps is determined exclusively by the rates of ion binding from either side of the membrane, i.e. by the transmembrane electrochemical gradient. If the c-ring is coupled to F_1, however, the free energies of ATP synthesis or hydrolysis, which depend on the concentrations of reactants and products (i.e. the phosphorylation potential), also contribute to determine the preferred direction of rotation. Excess amounts of ATP will strongly favor hydrolysis and drive the c-ring clockwise, resulting in accumulation of ions on the P-side. By contrast, depletion of ATP, and a sufficient supply of ADP and P_i, allows ions to permeate downhill, and the resulting counter-clockwise rotation of the c-ring drives the synthesis and release of ATP.

It is this context that we proceed to analyze the functional implications of the F/V-hybrid ring of the *A. woodii* ATP synthase, relative to an enzyme with a prototypical c_{11} ring. Specifically, we formulated two plausible free-energy landscapes designed to encompass the series of microscopic states and competing processes proposed to underlie the rotary mechanism (Fig. 9a); these are largely based on experimental and computational observations, including those reported here. We then used two complementary kinetic-modeling algorithms (Methods) to determine what these energy landscapes imply in regard to the ability of either enzyme to synthesize ATP, driven by an ion gradient, or to create and sustain a gradient, driven by ATP hydrolysis.

Both these analyses shows that ATP synthesis is viable in the *A. woodii* enzyme, either from a thermodynamic or a kinetic standpoint, in spite of the V-type c-subunit inserted in the c-ring. If, mimicking a voltage-clamp electrophysiological experiment, we initially set a sufficient Na^+ electrochemical gradient (30-fold), and provide sustained amounts of ADP (2 or 10 mM) and P_i (10 mM), the model yields a sizeable ATP output (70 mM) when equilibrium is ultimately reached (Fig. 9b). The amount of ATP produced by the *A. woodii* enzyme, however, smaller than that synthesized by an equivalent enzyme with a canonical homomeric c_{11} ring (5–13% in these conditions), all else being equal (Fig. 9b). That is, due to the missing binding site, the *A. woodii* enzyme is less able to dissipate the Na^+ gradient and therefore, from a thermodynamical standpoint, it is a slightly less productive ATP synthase. From a kinetic standpoint, the impact of the V-type c-subunit appears to also small

(Fig. 9d). As mentioned, the *A. woodii* model features an additional energetic barrier encountered when the c_1 subunit crosses the a/c interface. However, this barrier is much lower than those limiting the rotation rate when the enzyme functions in synthesis, i.e. those associated with the rotational stepping of the c-ring, which are uphill in energy (Methods, equation 10).

Because rotary ATPases are reversible enzymes, these observations raise the question of whether the V-type c-subunit would make the *A. woodii* enzyme a more capable ion pump than one with a homomeric c_{11} ring. The models used above, now examined in conditions that favor ATP hydrolysis, suggest this is indeed the case. If a null electrochemical gradient is initially set, along with sustained ATP and $[Na^+]_N$ concentrations (2 mM and 10 mM, respectively), Na^+ is progressively accumulated by both enzymes on the P-side of the membrane, as the concentrations of ADP and P_i raise (Fig. 9c). At equilibrium, however, the Na^+ gradient built up by the *A. woodii* ATP synthase (~30 fold) is significantly greater than that produced by the enzyme with a prototypical c_{11} ring (17% in these conditions) (Fig. 9c). Because the rotational displacements are considerably now faster than in synthesis (Methods, equation 11), the impact of the V-type c-subunit on the overall rotation kinetics is more apparent (Fig. 9d), but clearly not critical (~2-fold in our model).

In summary, this kinetic-modeling analysis indicates that the impact of the V-type double-hairpin c_1 subunit on the functionality of the *A. woodii* ATP synthase is not negligible but modest, explaining why this enzyme is the primary source of ATP in this organism. Our analysis also indicates, interestingly, that the V-type c-subunit embedded in the *A. woodii* c-ring would increase the thermodynamic capacity of the enzyme to generate an ion gradient, if driven by ATP hydrolysis, although this capacity would be maximally realized more slowly than with a prototypical c-ring. Although this observation is not necessarily relevant to the physiology of this acetogenic bacterium, it does have broader implications. By extension, it seems plausible that the evolutionary driving force behind the c-subunit gene duplication and loss of multiple binding sites that is often seen in the rotor rings of eukaryotic V-type ATPases is precisely to maximize the thermodynamic capacity of these enzymes to sustain robust, slowly-changing ion gradients, for a limited ATP input, such as those across the membranes of intracellular compartments.

Discussion

The high-resolution crystal structure of the *A. woodii* c-subunit ring establishes the existence of heteromeric c-rings in the rotary ATPase family, and provides unequivocal structural evidence for the Na^+ dependence of the *A. woodii* ATP synthase. Moreover, the structure shows that c-subunits with distinct transmembrane topologies and ion-binding site configurations can form functional assemblies. The *A. woodii* ring consists of nine single-hairpin c-subunits, each harboring a Na^+-binding site, and one double-hairpin c-subunit, with one additional site and one vacancy. While such heteromeric rotors with missing ion-binding sites are rare in bacteria, they are typical of eukaryotic V-type ATPases, e.g. in *S. cerevisiae* and in humans. To investigate whether such variations might reflect a functional adaptation, we dissected the microscopic rotary mechanism of the *A. woodii* c-ring via computer simulations and free-energy calculations. The results reveal a mechanism that is

largely comparable to that of conventional homomeric c-rings, albeit with slightly altered thermodynamic and kinetic characteristics. In particular, the V-type double-hairpin c-subunit diminishes the extent to which the sodium-motive-force may be harnessed for ATP production, but this effect does not appear to be functionally critical. An important related observation of broader implications is that the V-type c-subunit also increases the thermodynamic capacity of the enzyme to create or sustain an electrochemical gradient, relative to an equivalent enzyme with a canonical c-ring of the same size. Such an effect would be amplified if multiple V-type subunits were assembled into the c-ring, as found in vacuolar and plasma-membrane ATPases. Our observations thus suggest that adaptations in the membrane rotor have contributed to the structural-functional evolutionary path from prokaryotic ATP synthases to eukaryotic ATPases. By duplicating the c-subunit genes, the structural stability of the resulting c-rings is actually enhanced, for entropic reasons, thus making the loss of ion-binding sites much more tolerable than for single-hairpin homomeric c-rings. We propose that such adaptations have led to c-ring architectures that are inherently better suited for generation of robust ion gradients than for ATP production. The structure of the *A. woodii* ring appears to provide a glimpse into this evolutionary path.

Methods

Cell growth and protein purification

Acetobacterium woodii (DSM 1030) was grown in a 20-liter fermenter to an optical density of ~2.5 for about 20 h, as previously described[43], using 20 mM fructose as carbon source. Washed membrane vesicles[32] were adjusted to a protein concentration of 20 mg/ml in buffer A (50 mM Tris/HCl, pH 7.5; 50 mM NaCl; 5 mM $MgCl_2$) and solubilized with 2% (w/v) *n*-dodecyl-β-D-maltopyranoside (DDM) for 1 h at 4°C. The solubilized protein was collected by ultracentrifugation at 350,000 g for 15 min at 4°C and supplemented with 50 mM $MgCl_2$. The ATP synthase was enriched using an ATPase-activity controlled polyethylene glycol (PEG)-precipitation on ice. The 4–10% (w/v) PEG 6000-containing fraction was centrifuged at 8,000 g for 20 min at 4°C and the ATP synthase-containing pellet was solubilized in buffer B (20 mM Tris/HCl, pH 7.5; 100 mM NaCl; 5 mM EDTA; 0.05% DDM). For c-ring extraction, the sample was diluted to 5 mg/ml, solubilized with 1% (w/v) *N*-lauroylsarcosine at room temperature (RT) for 1 h, followed by a 10 min incubation at 68°C. A saturated ammonium sulfate solution (=100%, in 50 mM Tris/HCl, pH 8.0) was added to 68%, incubated for 20 min at RT and centrifuged at 8,000 g for 20 min. The supernatant was sterile filtered through a 0.2 μm filter (Sarstedt, Nümbrecht, Germany) and dialyzed against buffer C (20 mM Tris/HCl, pH 7.5; 50 mM NaCl). The c-ring was further purified using hydroxyapatite (BioGel HT; Bio-Rad, Munich, Germany) and sucrose density gradient centrifugation (5–35% sucrose in 20 mM Tris/HCl, pH 7.5; 50 mM NaCl; 0.1% *n*-decyl-β-D-maltopyranoside; 220,000 g, 21 h, 10°C). The sample was dialyzed against buffer C for 3 days and concentrated to approximately 4 mg/ml using an Amicon centrifugal filter device with a molecular weight cut-off of 10,000 (Millipore GmbH, Schwalbach, Germany) and stored at 4°C.

3D crystallization and structure determination

Before crystallization, 3% (w/v) *n*-heptyl-β-D-thioglucopyranoside (Affymetrix GmbH, Munich, Germany) was added to the c-ring sample and incubated over night at room temperature, followed by a 10 min incubation at 60°C and another hour at room temperature. The protein was mixed in a 1:1 ratio with buffer D (100 mM sodium acetate, pH 4.5; 9% (v/v) PEG 400; 20 mM $MnCl_2$) and crystallization was accomplished using a vapor diffusion hanging drop method in a 24-well plate with 500 µl reservoir (100 mM sodium acetate, pH 4.5; 9% (v/v) PEG 400) at 12°C in 4 days. After the crystals reached their final size, the PEG 400 concentration was gradually increased from 9 to 40% (v/v) within 48 hours and the crystals were flash frozen in liquid nitrogen. Approximately 1,000 crystals were screened at beamlines PX-II X10SA of the Swiss Light Source (SLS) in Villigen, Switzerland, and ID23.1, ID23.2 and ID29 of the European Synchrotron Radiation Facility (ESRF) in Grenoble, France. The final dataset used for this work (Supplementary Table 1) was collected at 100 K at microfocus beamline ID23.2 of the ESRF. The data was processed using XDS[44] and the structure was determined by molecular replacement with PHASER[45], using an adapted structure of the c_{11} ring from *Ilyobacter tartaricus* (PDB 1YCE) as a search model. The unit cell, in the $P4_32_12$ space group, comprises eight c-rings, with one c-ring as the asymmetric unit (Supplementary Fig. 4). Iterative rounds of model building into the $2F_{obs} - F_{calc}$ and $F_{obs} - F_{calc}$ electron-density maps, which were clearly traceable, were carried out with COOT[46], and the resulting model was refined with PHENIX[47]. The final refined structure has no Ramachandran outliers. The final atomic coordinates are deposited in the Protein Data Bank, with accession code 4BEM.

Atomic force microscopy and image analysis

The unprocessed AFM image used in this study was obtained as described previously[22], and analyzed applying a different classification approach and recent software versions. Firstly, the image was processed using Nanoscope V software (DI–Veeco, Santa Barbara, CA, USA). A gallery of 260 c-rings viewed from the periplasmic side was created in BOXER[48] applying a manual particle picking procedure and further classification in IMAGIC[49]. Particles were divided into 5 classes, which are used in the further analysis. 3D representations of the class averages were produced in DINO3D (http://www.dino3d.org). Cross-section profiles of the c-ring class averages were created using ImageJ[50].

Other biochemical methods

Protein concentrations were determined with the bicinchoninic acid method according to Pierce (Rockford, IL, USA), with bovine serum albumin as a standard. SDS-PAGE was performed as described previously[51] and all gels were silver-stained[52]. ATPase activity was determined by the coupled spectrophotometric assay[53].

Simulation systems and specifications

Molecular dynamcs (MD) simulations were calculated with NAMD 2.7[54] and the all-atom CHARMM27/CMAP force field[55,56]. All simulations were carried out at constant temperature (298 K) and pressure (1 atm) using a Langevin thermostat/barostat, and with periodic boundary conditions. Electrostatic interactions were computed using the particle-

mesh Ewald algorithm, with a 12-Å real-space cut-off; van der Waals interactions were truncated also at 12 Å. The c-ring from *Acetobacterium woodii* was simulated either in a hydrated 1-palmitoyl-2-oleoyl-*sn*-glycero-3-phosphocholine (POPC) lipid membrane, or in a solution consisting of 2-methyl-2,4-pentanediol (MPD) and water. The atomic coordinates for the c-ring at the beginning of the simulations were those in the crystal structure at 2.1-Å resolution. The Na^+ ions and crystallographic water molecules identified in the structure were also included. Both membrane/water and MPD/water systems were prepared as described previously[57,14]. The membrane system includes 233 POPC and 18,448 water molecules, in an orthorhombic box 100 × 100 × 95.6 Å. The MPD system includes 750 MPD and 12,363 water molecules, in a cubic box of 86.4 Å, i.e. approximately a 30:70 volume ratio. In both systems, nine K^+ ions were added to neutralize the net charge of the system. After the initial set-up, the protein-lipid and protein-MPD interfaces were equilibrated via simulations of 80 ns and 200 ns, respectively. During the equilibrations, the dynamics of the c-ring was restricted using a combination of position, distance and conformational restraints, which were gradually released.

Simulations of spontaneous Na^+ unbinding and rebinding

To characterize the dynamics of the c-ring and study the mechanism of Na^+ unbinding, two unrestrained simulations of 350 ns each were calculated for the MPD system, and one simulation of 260 ns was calculated for the POPC system. Both MPD simulations revealed Na^+ dissociation events. A third simulation of 200 ns was also calculated to study the mechanism of Na^+ rebinding. This last simulation was initiated 45 ns after one of the Na^+ dissociation events, when the unbound Na^+ approached the c-ring binding site (within 25 Å) from which it originated, after diffusing across the simulation box. To preclude the ion from diffusing away from the c-ring, a harmonic soft-wall (k = 15 kcal/mol/Å^2) was introduced, at a distance of 20 Å from the carboxylic group (Glu62) that coordinates the ion in the binding site. This confinement effect is equivalent to that of a ~100 mM NaCl concentration, and does not interfere with the ion-protein interaction. Additional simulations of the c-ring in MPD/water were prepared to assess whether the c_1 subunit may bind Na^+ in a hydrophilic environment. Na^+ was modeled into this site in a hypothetical coordination network optimized through a 5-ns simulation with ion-protein distance restraints, namely to Gln129(Oε1), T80(Oγ and V77(O) (each restraint consisted of a harmonic potential flat-bottomed up to 3 Å and with k = 15 kcal/mol/Å^2). Five independent simulations were then carried out without restraints.

Free-energy calculations

A series of enhanced-sampling MD simulations of the c-ring in MPD/water were designed to gain insights into the energetics of two key elements in the proposed rotary mechanism. First, to assess the putative role of a conserved arginine in TM4 of subunit-a in precluding direct ion hopping between the two binding sites at the a/c interface, we extracted a snapshot from one of the unbiased simulations of the c-ring in MPD/water after a spontaneous Na^+ unbinding event, and the exposed Glu62 side-chain in the empty site was allowed to form an ion-pair with a guanidinium cation (GND^+) added to the buffer. The free-energy cost of transferring a Na^+ ion to this unlocked, GND^+-paired site from an adjacent locked binding site was then computed using the Free-Energy Perturbation method[54]. To model the

configuration of the unlocked, GND^+-paired site bound to Na^+, we used the same procedure described above for the c_1 subunit. The transfer free energy was evaluated in both directions, using a decoupling/re-coupling scheme comprising 40 intermediates. Each intermediate simulation consisted of a 100-ps equilibration followed by 1 ns of averaging time. The GND^+-carboxyl ion-pair was maintained using a distance restraint (a harmonic potential flat-bottomed up to 3.8 Å and with k = 15 kcal/mol/Å^2); the effect of this restraint on the transfer free energy value is < 0.1 kcal/mol.

Free-energy calculations were also used to evaluate the plausibility of the proposed switch of interactions between the subunit-a arginine and either of the two c-ring binding sites exposed the a/c interface (when both are concurrently ion-free). The c-ring was prepared in three configurations, namely (a) with two adjacent binding sites in $c_{2/3}/c_{2/3}$ interfaces in the ion-free state, (b) with the binding site in the $c_1/c_{2/3}$ interface in the ion-free state, and (c) with the binding site in the $c_{2/3}/c_1$ interface in the ion-free state. A GND^+ cation was again added to the MPD/water buffer in all systems and allowed to form an ion-pair with one of the exposed Glu62 side-chains. The Adaptive Biasing Force method[58] was then used to simulate the reversible exchange of GND^+ interactions with (a) either of the two ion-free $c_{2/3}/c_{2/3}$ binding sites, (b) the ion-free $c_{2/3}/c_1$ site and the c_1 site, and (c) the c_1 site and the ion-free $c_{2/3}/c_1$ site. Two reaction coordinates were employed to bias the sampling in these simulations, namely the distances between the center-of-mass of GND^+ and the carboxylate/carboxamide groups of the glutamate/glutamine side-chains in the c-subunits involved. The range of distances explored was 3 to 18 Å. The diffusion of the GND^+ ion in the direction perpendicular to the membrane plane was confined to a region 10 Å in width, centered at the binding sites. Two-dimensional and one-dimensional free-energy landscapes were obtained from each of these simulations, which lasted (a) 150 ns, (b) 280 ns, and (c) 280 ns, respectively. The sampling of the landscape was carried in bins of 0.25 Å for each reaction coordinate; at each bin, 1,000 samples were collected before applying the biasing force.

Kinetic model of the coupled F_1F_o enzyme

A kinetic model was designed to evaluate the influence of the c_1 subunit on the thermodynamic capacity and rotation rate of the *A. woodii* ATP synthase under conditions that favor either ATP synthesis, driven by downhill ion permeation, or ATP hydrolysis, resulting in the generation of an ion gradient. The results were compared with an analogous model for a canonical F-type homomeric c-ring with 11 subunits and no missing binding sites. Both kinetic models are based on the premise that the rotation of the of the c-ring can be described by a series of discrete rotational states Ω_i, each of which is uniquely defined by the two specific c-subunits that are concurrently exposed to subunit-a, denoted by $\mathbf{S_P}$, $\mathbf{S_N}$; all other sites, denoted by S_M, face the lipid membrane. Therefore, the 11 rotational states of the a/c complex would be:

$$
\begin{array}{lcccccccccccc}
\Omega_1 & = & \mathbf{S_P} & \mathbf{S_N} & S_M & S_M & S_M & S_M & S_M & S_M & S_M & S_M \\
\Omega_2 & = & S_M & \mathbf{S_P} & \mathbf{S_N} & S_M & S_M & S_M & S_M & S_M & S_M & S_M \\
\Omega_3 & = & S_M & S_M & \mathbf{S_P} & \mathbf{S_N} & S_M & S_M & S_M & S_M & S_M & S_M \\
\cdots & \cdots & \cdots & \cdots & & & & & & & & \\
\Omega_{11} & = & \mathbf{S_N} & S_M & S_M & S_M & S_M & S_M & S_M & S_M & S_M & \mathbf{S_P}
\end{array}
$$

Note that this specific numbering reflects counter-clockwise rotations. Also note that the model allows transitions between adjacent rotational states only, and thus state Ω_{11} is followed/preceded by Ω_1. In addition, we postulate that each of these rotational states comprises the series of sub-states depicted in Fig. 6. Specifically, ion-binding sites (i.e. those featuring a glutamate residue) exposed to the membrane (S_M) are assumed to be locked in the Na^+-bound state (E^+), while those exposed to subunit-a (S_P, S_N) are either Na^+-bound (E^+), Na^+-free (E), or engaged to the key arginine side-chain in subunit-a (E^R). In the *A. woodii* model, the site within the c_1 subunit is always Na^+-free (Q), but it can also engage the arginine in subunit-a (Q^R). The connectivity between these sub-states is pre-defined (according to Fig. 6), but all transitions are reversible. A partial sequence of sub-states for the *A. woodii* model is, for example (the two c-subunits at $\mathbf{S_P}$ and $\mathbf{S_N}$ are again indicated in bold):

$$
\begin{array}{lcccccccccccc}
\Omega_{1,1} & = & \mathbf{E^R} & \mathbf{E^+} & E^+ & Q & E^+ & E^+ & E^+ & E^+ & E^+ & E^+ & E^+ \\
\Omega_{1,2} & = & \mathbf{E^R} & \mathbf{E} & E^+ & Q & E^+ & E^+ & E^+ & E^+ & E^+ & E^+ & E^+ \\
\Omega_{1,3} & = & \mathbf{E} & \mathbf{E^R} & E^+ & Q & E^+ & E^+ & E^+ & E^+ & E^+ & E^+ & E^+ \\
\Omega_{1,4} & = & \mathbf{E^+} & \mathbf{E^R} & E^+ & Q & E^+ & E^+ & E^+ & E^+ & E^+ & E^+ & E^+ \\
\Omega_{2,1} & = & E^+ & \mathbf{E^R} & \mathbf{E^+} & Q & E^+ & E^+ & E^+ & E^+ & E^+ & E^+ & E^+ \\
\Omega_{2,2} & = & E^+ & \mathbf{E^R} & \mathbf{E} & Q & E^+ & E^+ & E^+ & E^+ & E^+ & E^+ & E^+ \\
\Omega_{2,3} & = & E^+ & \mathbf{E} & \mathbf{E^R} & Q & E^+ & E^+ & E^+ & E^+ & E^+ & E^+ & E^+ \\
\Omega_{2,4} & = & E^+ & \mathbf{E^+} & \mathbf{E^R} & Q & E^+ & E^+ & E^+ & E^+ & E^+ & E^+ & E^+ \\
\Omega_{3,1} & = & E^+ & E^+ & \mathbf{E^R} & \mathbf{Q} & E^+ & E^+ & E^+ & E^+ & E^+ & E^+ & E^+ \\
\Omega_{3,2} & = & E^+ & E^+ & \mathbf{E} & \mathbf{Q^R} & E^+ & E^+ & E^+ & E^+ & E^+ & E^+ & E^+ \\
\Omega_{3,3} & = & E^+ & E^+ & \mathbf{E^+} & \mathbf{Q^R} & E^+ & E^+ & E^+ & E^+ & E^+ & E^+ & E^+ \\
\Omega_{4,1} & = & E^+ & E^+ & E^+ & \mathbf{Q^R} & \mathbf{E^+} & E^+ & E^+ & E^+ & E^+ & E^+ & E^+ \\
\Omega_{4,2} & = & E^+ & E^+ & E^+ & \mathbf{Q^R} & \mathbf{E} & E^+ & E^+ & E^+ & E^+ & E^+ & E^+ \\
\Omega_{4,3} & = & E^+ & E^+ & E^+ & \mathbf{Q} & \mathbf{E^R} & E^+ & E^+ & E^+ & E^+ & E^+ & E^+ \\
\Omega_{5,1} & = & E^+ & E^+ & E^+ & Q & \mathbf{E^R} & \mathbf{E^+} & E^+ & E^+ & E^+ & E^+ & E^+ \\
\cdots & \cdots & \cdots & & & & & & & & & &
\end{array}
$$

The profiles shown in Fig. 9a represent graphically the relative free-energy values and kinetic barriers between these rotational states and sub-states; these reflect available experimental measurements and molecular-dynamics simulation data, and also account for the effect of the sodium-motive-force and the phosphorylation potential. Specifically, the energy cost of Na^+ unbinding from the S_N site is:

$$\Delta G(\mathrm{E/Q^R, E^+ \rightarrow E/Q^R, E}) = -\Delta G_\mathrm{b} - \frac{F\Delta\Psi}{2} + k_\mathrm{B}T \ln\left[\mathrm{Na^+}\right]_\mathrm{N} \quad (1)$$

where $\Delta G_b \sim -5.5$ kcal/mol is the standard Na^+ binding affinity at pH 7 (unpublished experimental results), and $[Na^+]_N$ is the Na^+ concentration on the N-side of the membrane. $\Delta\Psi$ is the electrostatic potential applied across the membrane (as in a voltage-clamp experiment), F and k_B are the Faraday and Boltzmann constants, and T the temperature (300 K). Similarly, the free-energy gain associated with Na^+ binding S_P site is:

$$\Delta G(\mathrm{E, E/Q^R \rightarrow E^+, E/Q^R}) = \Delta G_\mathrm{b} - \frac{F\Delta\Psi}{2} - k_\mathrm{B}T \ln\left[\mathrm{Na^+}\right]_\mathrm{P} \quad (2)$$

Based on the free-energy simulations summarized in Fig. 8, for the arginine-switch step:

$$\Delta G(\mathrm{E^R, E} \rightarrow \mathrm{E, E^R}) = 0 \quad (3)$$

$$\Delta G(\mathrm{E^R, Q} \rightarrow \mathrm{E, Q^R}) = -\Delta G(\mathrm{Q^R, E} \rightarrow \mathrm{Q, E^R}) = 4.6\ \mathrm{kcal/mol} \quad (4)$$

Lastly, each rotational step entails a free-energy cost in the counter-clockwise direction (or gain, if clockwise), due to the mechanical coupling between the c-ring and the catalytic domain:

$$\Delta G(\Omega_i \rightarrow \Omega_{i+1}) = -\frac{3}{11}\left\{\Delta G^0 + k_\mathrm{B}T \ln \frac{[\mathrm{ADP}][\mathrm{P_i}]}{[\mathrm{ATP}]}\right\} \quad (5)$$

where $\Delta G^0 \sim -7.3$ kcal/mol is the standard free energy of ATP hydrolysis at pH 7[59]. Note that the assumption implicit in equation 5 is that the cost or gain associated with ATP synthesis or hydrolysis is uniformly distributed over all rotational steps; this is consistent with the notion of an elastic transmission between the F_1 and F_o domains[60].

The relative free-energy values defined in equations 1–5 determine the transition rates between adjacent sub-states in the rotational cycle[61]. For example, for Na^+ unbinding from and rebinding to the S_N site, these rates are, respectively:

$$\begin{aligned} k(\mathrm{E/Q^R, E^+} \rightarrow \mathrm{E/Q^R, E}) &= \kappa \exp\left\{\tfrac{\Delta G_\mathrm{b} + F\Delta\Psi/2}{2k_\mathrm{B}T}\right\} \\ k(\mathrm{E/Q^R, E} \rightarrow \mathrm{E/Q^R, E^+}) &= \kappa \exp\left\{\tfrac{-\Delta G_\mathrm{b} - F\Delta\Psi/2}{2k_\mathrm{B}T}\right\} [\mathrm{Na^+}]_\mathrm{N} \end{aligned} \quad (6\text{–}7)$$

Note only the latter is dependent on $[Na^+]_N$. Likewise, for the S_P site:

$$\begin{aligned} k(\mathrm{E, E/Q^R} \rightarrow \mathrm{E^+, E/Q^R}) &= \kappa \exp\left\{\tfrac{-\Delta G_\mathrm{b} + F\Delta\Psi/2}{2k_\mathrm{B}T}\right\} [\mathrm{Na^+}]_\mathrm{P} \\ k(\mathrm{E^+, E/Q^R} \rightarrow \mathrm{E, E/Q^R}) &= \kappa \exp\left\{\tfrac{\Delta G_\mathrm{b} - F\Delta\Psi/2}{2k_\mathrm{B}T}\right\} \end{aligned} \quad (8\text{–}9)$$

And for the transition between rotational steps:

$$\begin{aligned} k(\Omega_i \rightarrow \Omega_{i+1}) &= \kappa' \exp\left\{\tfrac{3}{11}\tfrac{\Delta G^0}{2k_\mathrm{B}T}\right\} [\mathrm{ADP}]^{3/11}[\mathrm{P_i}]^{3/11} \\ k(\Omega_i \rightarrow \Omega_{i-1}) &= \kappa' \exp\left\{-\tfrac{3}{11}\tfrac{\Delta G^0}{2k_\mathrm{B}T}\right\} [\mathrm{ATP}]^{3/11} \end{aligned} \quad (10\text{–}11)$$

Note that the rate of counter-clockwise rotations (equation 10) is accelerated by [ADP] and $[P_i]$, while that of clockwise rotations (equation 11) is enhanced by [ATP]. The exponential pre-factors κ and κ' in equations 6–11 can be thought as the intrinsic transition rates in the absence of a driving force. For simplicity, we used $\kappa = 1$, and $\kappa' = 10^{-6}$, that is, the assumed *kinetic barrier* between rotational states is effectively ~8 kcal/mol greater than for between sub-states. We believe this assumption is justified given that rotational transitions involve a large-scale reconfiguration of the c-ring interface with both subunit-a and the lipid membrane, and possibly a conformational change within subunit-a as well. By contrast, transitions between sub-states entail only structurally localized changes, coupled to the

exchange of Na^+ with the bulk solution, which are likely to be kinetically faster under physiological conditions.

Two complementary algorithms were utilized to characterize the multi-state kinetic model just described. In the first algorithm, initial concentration conditions are set for Na^+, on either side of the membrane, and for ATP, ADP and P_i, and system of interdependent differential equations describing the time-evolution of all species in the model is resolved so as to determine the concentrations of at equilibrium[62]. That is, the model predicts how the thermodynamic driving forces associated with an initial chemical imbalance are transduced to yield one or other output, leaving aside kinetic effects. In the second approach, the time-evolution of the rotary mechanism is explicitly analyzed, for the same out-of-equilibrium initial conditions, using a kinetic Monte-Carlo algorithm[63]. To do so, the cycle is initiated in a sub-state chosen at random, and evolved through a stochastic, iterative procedure, according to the instantaneous probability a forward or a backward transition, P^+ or P^-. These probabilities are derived from the set of rates defined in e.g. equations 6–11, i.e.:

$$P^+ = 1 - P^- = \frac{k^+}{k^+ + k^-} \quad (12)$$

To determine whether the cycle proceeds forward or backward at a given time, a random number R uniformly distributed between 0 and 1 is generated at each iteration; if $R < P^+$ the cycle evolves forward and otherwise backward. Either way, the simulated time increases by:

$$\Delta t = \frac{-\ln(r)}{k^+ + k^-} \quad (13)$$

where r is also a random number uniformly distributed between 0 and 1, also generated at each iteration. The outcome of this iterative procedure is rotational stochastic trajectory. Initially, these trajectories reflect a preferential directionality, but at equilibrium clockwise and counter-clockwise rotations balance each other.

Supplementary Material

Refer to Web version on PubMed Central for supplementary material.

Acknowledgments

We thank Vanessa Leone for sharing unpublished experimental data and models of the a/c complex, Janet Vonck for advice on single-particle analysis, and Fabrizio Marinelli for useful discussions. We also thank the staff of the Swiss Light Source (PXII) and the European Synchrotron Radiation Facility for their continuous support. This research was supported with funds from the Collaborative Research Center (SFB) 807 of the German Research Foundation (DFG) (T.M. and V.M.), the Cluster of Excellence ‘Macromolecular Complexes’ (DFG Project EXC 115) (T.M.), and the Division of Intramural Research at NHLBI/NIH (J.D.F.-G.).

References

1. Junge W, Nelson N. Nature’s rotary electromotors. Science. 2005; 308:642–644. [PubMed: 15860615]

2. Fillingame RH. Coupling H^+ transport and ATP synthesis in F_1F_o-ATP synthases: glimpses of interacting parts in a dynamic molecular machine. J Exp Biol. 1997; 200:217–224. [PubMed: 9050229]
3. Rocha-Facanha A, de Meis L. Reversibility of H^+-ATPase and H^+-pyrophosphatase in tonoplast vesicles from maize coleoptiles and seeds. Plant Physiol. 1998; 116:1487–1495. [PubMed: 9536067]
4. Hirata T, Nakamura N, Omote H, Wada Y, Futai M. Regulation and reversibility of vacuolar H^+-ATPase. J Biol Chem. 2000; 275:386–389. [PubMed: 10617629]
5. Pogoryelov D, et al. Engineering rotor ring stoichiometries in the ATP synthase. Proc Natl Acad Sci USA. 2012; 109:E1599–1608. [PubMed: 22628564]
6. Walker JE. The ATP synthase: the understood, the uncertain and the unknown. Biochem Soc Trans. 2013; 41:1–16. [PubMed: 23356252]
7. Mayer F, Müller V. Adaptations of anaerobic archaea to life under extreme energy limitation. FEMS Microbiol Rev. 201310.1111/1574-6976.12043
8. Forgac M. Vacuolar ATPases: rotary proton pumps in physiology and pathophysiology. Nat Rev Mol Cell Biol. 2007; 8:917–929. [PubMed: 17912264]
9. Nelson N. Structural conservation and functional diversity of V-ATPases. J Bioenerg Biomembr. 1992; 24:407–414. [PubMed: 1400285]
10. Stock D, Leslie AG, Walker JE. Molecular architecture of the rotary motor in ATP synthase. Science. 1999; 286:1700–1705. [PubMed: 10576729]
11. Vonck J, et al. Molecular architecture of the undecameric rotor of a bacterial Na^+-ATP synthase. J Mol Biol. 2002; 321:307–316. [PubMed: 12144787]
12. Meier T, Polzer P, Diederichs K, Welte W, Dimroth P. Structure of the rotor ring of F-type Na^+-ATPase from *Ilyobacter tartaricus*. Science. 2005; 308:659–662. [PubMed: 15860619]
13. Pogoryelov D, Yildiz Ö, Faraldo-Gómez JD, Meier T. High-resolution structure of the rotor ring of a proton-dependent ATP synthase. Nat Struct Mol Biol. 2009; 16:1068–1073. [PubMed: 19783985]
14. Symersky J, et al. Structure of the c_{10} ring of the yeast mitochondrial ATP synthase in the open conformation. Nat Struct Mol Biol. 2012; 19:485–491. [PubMed: 22504883]
15. Pogoryelov D, Yu J, Meier T, Vonck J, Dimroth P, Muller DJ. The c_{15} ring of the *Spirulina platensis* F-ATP synthase: F_1/F_o symmetry mismatch is not obligatory. EMBO Rep. 2005; 6:1040–1044. [PubMed: 16170308]
16. Watt IN, Montgomery MG, Runswick MJ, Leslie AG, Walker JE. Bioenergetic cost of making an adenosine triphosphate molecule in animal mitochondria. Proc Natl Acad Sci USA. 2010; 107:16823–16827. [PubMed: 20847295]
17. Murata T, Yamato I, Kakinuma Y, Leslie AG, Walker JE. Structure of the rotor of the V-type Na^+-ATPase from *Enterococcus hirae*. Science. 2005; 308:654–659. [PubMed: 15802565]
18. Kibak H, Taiz L, Starke T, Bernasconi P, Gogarten JP. Evolution of structure and function of V-ATPases. J Bioenerg Biomembr. 1992; 24:415–424. [PubMed: 1400286]
19. Arai H, Terres G, Pink S, Forgac M. Topography and subunit stoichiometry of the coated vesicle proton pump. J Biol Chem. 1988; 263:8796–8802. [PubMed: 2897963]
20. Flannery AR, Graham LA, Stevens TH. Topological characterization of the c, c′, and c″ subunits of the vacuolar ATPase from the yeast *Saccharomyces cerevisiae*. J Biol Chem. 2004; 279:39856–39862. [PubMed: 15252052]
21. Benlekbir S, Bueler SA, Rubinstein JL. Structure of the vacuolar-type ATPase from *Saccharomyces cerevisiae* at 11-Å resolution. Nat Struct Mol Biol. 2012; 19:1356–1362. [PubMed: 23142977]
22. Fritz M, et al. An intermediate step in the evolution of ATPases: a hybrid F_o-V_o rotor in a bacterial Na^+ F_1F_o ATP synthase. FEBS J. 2008; 275:1999–2007. [PubMed: 18355313]
23. Meier T, Matthey U, Henzen F, Dimroth P, Müller DJ. The central plug in the reconstituted undecameric c cylinder of a bacterial ATP synthase consists of phospholipids. FEBS Lett. 2001; 505:353–356. [PubMed: 11576527]

24. Oberfeld B, Brunner J, Dimroth P. Phospholipids occupy the internal lumen of the c ring of the ATP synthase of *Escherichia coli*. Biochemistry. 2006; 45:1841–1851. [PubMed: 16460030]
25. Pogoryelov D, et al. The oligomeric state of c rings from cyanobacterial F-ATP synthases varies from 13 to 15. J Bacteriol. 2007; 189:5895–5902. [PubMed: 17545285]
26. Schulz S, et al. A new type of Na^+-driven ATP synthase membrane rotor with a two-carboxylate ion-coupling motif. PLoS Biol. 2013; 11:e1001596. [PubMed: 23824040]
27. Leone V, Krah A, Faraldo-Gómez JD. On the question of hydronium binding to ATP-synthase membrane rotors. Biophys J. 2010; 99:L53–55. [PubMed: 20923632]
28. Preiss L, Yildiz Ö, Hicks DB, Krulwich TA, Meier T. A new type of proton coordination in an F_1F_o-ATP synthase rotor ring. PLoS Biol. 2010; 8:e000443.
29. Meier T, Krah A, Bond PJ, Pogoryelov D, Diederichs K, Faraldo-Gómez JD. Complete ion-coordination structure in the rotor ring of Na^+-dependent F-ATP synthases. J Mol Biol. 2009; 391:498–507. [PubMed: 19500592]
30. Krah A, Pogoryelov D, Langer JD, Bond PJ, Meier T, Faraldo-Gómez JD. Structural and energetic basis for H^+ versus Na^+ binding selectivity in ATP synthase F_o rotors. Biochim Biophys Acta. 2010; 1797:763–772. [PubMed: 20416273]
31. Schlegel K, Leone V, Faraldo-Gómez JD, Müller V. Promiscuous archaeal ATP synthase concurrently coupled to Na^+ and H^+ translocation. Proc Natl Acad Sci USA. 2012; 109:947–952. [PubMed: 22219361]
32. Fritz M, Müller V. An intermediate step in the evolution of ATPases: the F_1F_o-ATPase from *Acetobacterium woodii* contains F-type and V-type rotor subunits and is capable of ATP synthesis. FEBS J. 2007; 274:3421–3428. [PubMed: 17555523]
33. Preiss L, et al. The c-ring stoichiometry of ATP synthase is adapted to cell physiological requirements of alkaliphilic *Bacillus pseudofirmus* OF4. Proc Natl Acad Sci USA. 2013; 110:7874–7879. [PubMed: 23613590]
34. Pogoryelov D, Krah A, Langer JD, Yildiz Ö, Faraldo-Gómez JD, Meier T. Microscopic rotary mechanism of ion translocation in the F_o complex of ATP synthases. Nat Chem Biol. 2010; 6:891–899. [PubMed: 20972431]
35. Vik SB, Antonio BJ. A mechanism of proton translocation by F_1F_o ATP synthases by double mutants of the a subunit. J Biol Chem. 1994; 269:30364–30369. [PubMed: 7982950]
36. Junge W, Lill H, Engelbrecht S. ATP synthase: an electrochemical transducer with rotatory mechanics. Trends Biochem Sci. 1997; 22:420–423. [PubMed: 9397682]
37. Dong H, Fillingame RH. Chemical reactivities of cysteine substitutions in subunit a of ATP synthase define residues gating H^+ transport from each side of the membrane. J Biol Chem. 2010; 285:39811–39818. [PubMed: 20943664]
38. Krah A, Pogoryelov D, Meier T, Faraldo-Gómez JD. On the structure of the proton-binding site in the F_o rotor of chloroplast ATP synthases. J Mol Biol. 2010; 395:20–27. [PubMed: 19883662]
39. Jiang W, Fillingame RH. Interacting helical faces of subunits a and c in the F_1F_o ATP synthase of *Escherichia coli* defined by disulfide cross-linking. Proc Natl Acad Sci USA. 1998; 95:6607–6612. [PubMed: 9618459]
40. Hatch LP, Cox GB, Howitt SM. The essential arginine residue at position 210 in the a subunit of the *Escherichia coli* ATP synthase can be transferred to position 252 with partial retention of activity. J Biol Chem. 1995; 270:29407–29412. [PubMed: 7493977]
41. Valiyaveetil FI, Fillingame RH. On the role of Arg210 and Glu219 of subunit a in proton translocation by the *Escherichia coli* F_oF_1-ATP synthase. J Biol Chem. 1997; 272:32635–32641. [PubMed: 9405480]
42. Mitome N, Ono S, Sato H, Suzuki T, Sone N, Yoshida M. Essential arginine residue of the F_o-a subunit in F_oF_1-ATP synthase has a role to prevent the proton shortcut without c-ring rotation in the F_o proton channel. Biochem J. 2010; 430:171–177. [PubMed: 20518749]
43. Heise R, Muller V, Gottschalk G. Acetogenesis and ATP synthesis in *Acetobacterium woodii* are coupled via a transmembrane primary sodium-ion gradient. FEMS Microbiol Lett. 1993; 112:261–268.
44. Kabsch W. XDS. Acta Crystallogr D Biol Crystallogr. 2010; 66:125–132. [PubMed: 20124692]

45. McCoy AJ, Grosse-Kunstleve RW, Adams PD, Winn MD, Storoni LC, Read RJ. PHASER crystallographic software. J Appl Crystallogr. 2007; 40:658–674. [PubMed: 19461840]
46. Emsley P, Cowtan K. COOT: model-building tools for molecular graphics. Acta Crystallogr D Biol Crystallogr. 2004; 60:2126–2132. [PubMed: 15572765]
47. Zwart PH, et al. Automated structure solution with the PHENIX suite. Methods Mol Biol. 2008; 426:419–435. [PubMed: 18542881]
48. Ludtke SJ, Baldwin PR, Chiu W. EMAN: semiautomated software for high-resolution single-particle reconstructions. J Struct Biol. 1999; 128:82–97. [PubMed: 10600563]
49. van Heel M, Harauz G, Orlova EV, Schmidt R, Schatz M. A new generation of the IMAGIC image processing system. J Struct Biol. 1996; 116:17–24. [PubMed: 8742718]
50. Schneider CA, Rasband WS, Eliceiri KW. NIH Image to ImageJ: 25 years of image analysis. Nat Methods. 2012; 9:671–675. [PubMed: 22930834]
51. Schagger H, von Jagow G. Tricine-sodium dodecyl sulfate-polyacrylamide gel electrophoresis for the separation of proteins in the range from 1 to 100 kDa. Anal Biochem. 1987; 166:368–379. [PubMed: 2449095]
52. Nesterenko MV, Tilley M, Upton SJ. A simple modification of Blum's silver stain method allows for 30 minute detection of proteins in polyacrylamide gels. J Biochem Biophys Methods. 1994; 28:239–242. [PubMed: 8064118]
53. Neumann S, Matthey U, Kaim G, Dimroth P. Purification and properties of the F_1F_o ATPase of *Ilyobacter tartaricus*, a sodium ion pump. J Bacteriol. 1998; 180:3312–3316. [PubMed: 9642181]
54. Phillips JC, et al. Scalable molecular dynamics with NAMD. J Comp Chem. 2005; 26:1781–1802. [PubMed: 16222654]
55. MacKerell AD, et al. All-atom empirical potential for molecular modeling and dynamics studies of proteins. J Phys Chem B. 1998; 102:3586–3616. [PubMed: 24889800]
56. MacKerell AD, Feig M, Brooks CL. Improved treatment of the protein backbone in empirical force fields. J Am Chem Soc. 2004; 126:698–699. [PubMed: 14733527]
57. Staritzbichler R, Anselmi C, Forrest LR, Faraldo-Gómez JD. GRIFFIN: A Versatile Methodology for Optimization of Protein-Lipid Interfaces for Membrane Protein Simulations. J Chem Theor Comp. 2011; 7:1167–1176.
58. Henin J, Chipot C. Overcoming free energy barriers using unconstrained molecular dynamics simulations. J Chem Phys. 2004; 121:2904–2914. [PubMed: 15291601]
59. Atkins, PW. Physical Chemistry. 2. W.H. Freeman & Company; 1982.
60. Wachter A, et al. Two rotary motors in F-ATP synthase are elastically coupled by a flexible rotor and a stiff stator stalk. Proc Natl Acad Sci USA. 2011; 108:3924–3929. [PubMed: 21368147]
61. Kim YC, Wikstrom M, Hummer G. Kinetic models of redox-coupled proton pumping. Proc Natl Acad Sci USA. 2007; 104:2169–2174. [PubMed: 17287344]
62. Martinez-Forero I, Pelaez-Lopez A, Villoslada P. Steady state detection of chemical reaction networks using a simplified analytical method. PLoS One. 2010; 5:e10823. [PubMed: 20532219]
63. Voter, AF. Introduction to the kinetic Monte Carlo method. In: Sickafus, KE.; Kotomin, EA.; Uberuaga, BP., editors. Radiation Effects in Solids. Springer; Netherlands: 2007.
64. DeLeon-Rangel J, Ishmukhametov RR, Jiang W, Fillingame RH, Vik SB. Interactions between subunits a and b in the rotary ATP synthase as determined by cross-linking. FEBS Lett. 2013; 587:892–897. [PubMed: 23416299]

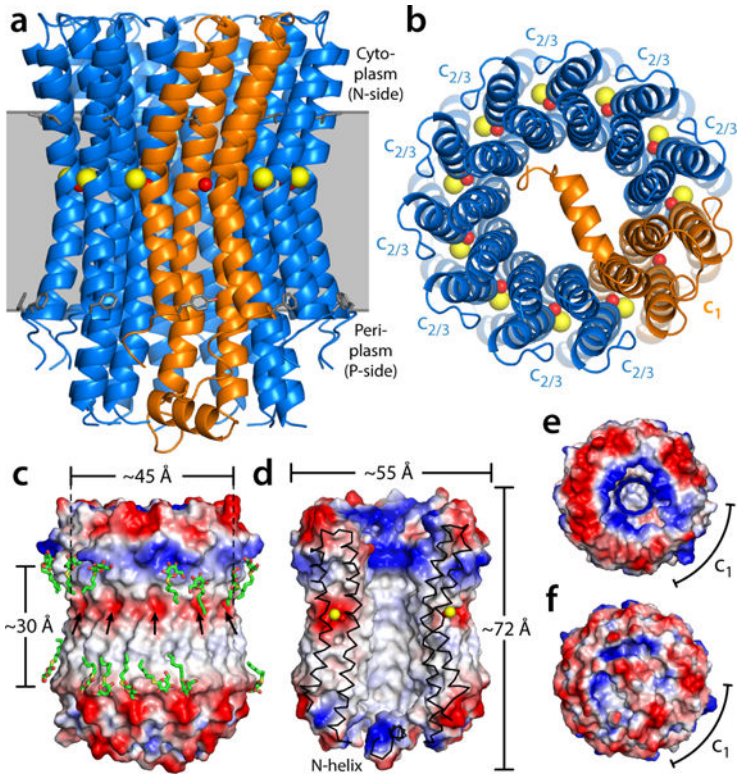

Figure 1.

Structure of the heteromeric c-ring from the *Acetobacterium woodii* ATP synthase. The ring is viewed (**a**) along the membrane plane and (**b**) from the periplasm, highlighting the two c-subunit topologies (blue and orange cartoons), as well as the bound Na^+ ions (yellow spheres) and the co-coordinating water molecules (red spheres). Note the site within subunit c_1 does not bind Na^+. Residues L55/F77 in $c_{2/3}$, and L72/L155/F94/Y177 in c_1 indicate the likely position of the ring within the membrane (gray). (**c**) Electrostatic potential at the outer surface of the c-ring, and (**d**) at the surface of the central hydrophobic pore. Detergent molecules (green) resolved in the electron density map are highlighted. Arrows indicate the position of the ion-binding sites. (**e**) Asymmetry of the electrostatic potential on the cytoplasmic face of the c-ring, where the central stalk binds. (**f**) The N-terminal extension of subunit c_1 occludes the central pore almost completely.

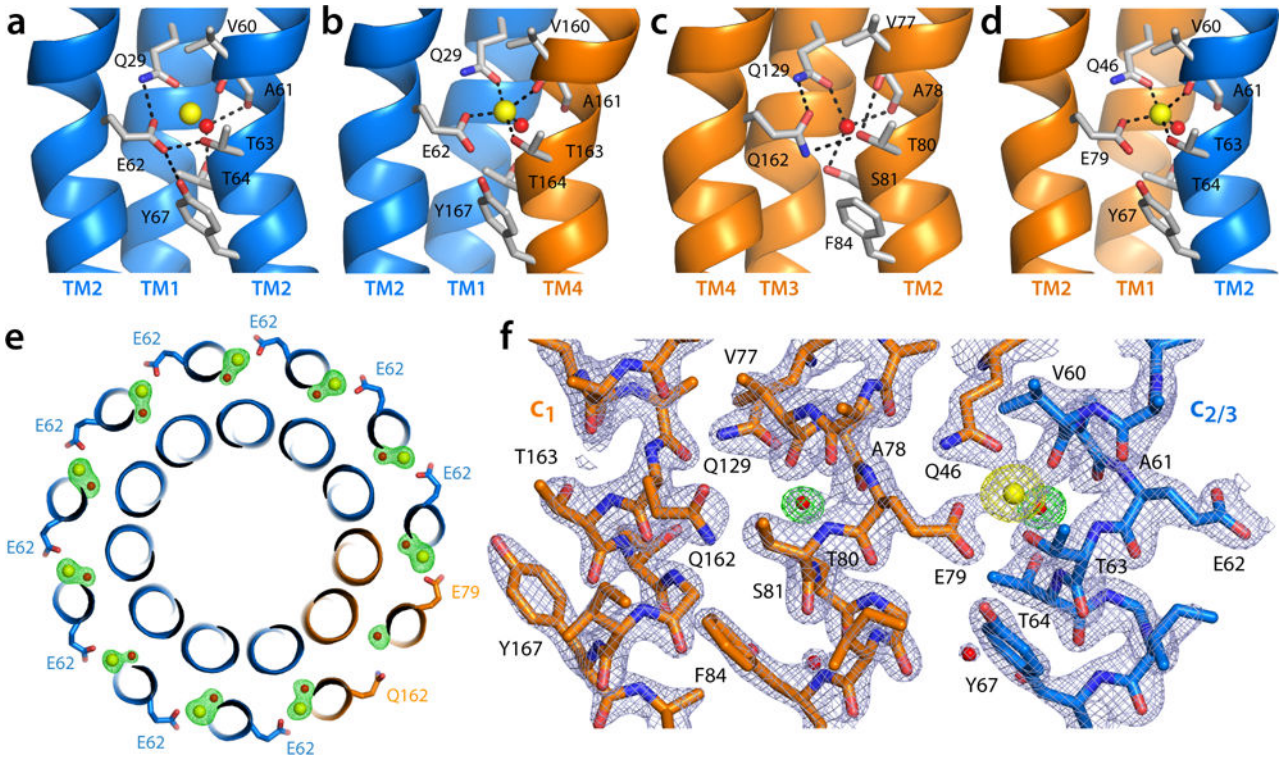

Figure 2.

Configuration of ion-binding sites in the *A. woodii* c-ring. (**a**) One of the eight Na^+-binding sites at the interfaces between $c_{2/3}$ subunits, viewed from the membrane. The protein residues (gray sticks) and water molecule (red sphere) coordinating the ion (yellow sphere) are highlighted. (**b** The Na^+-binding site at the $c_{2/3}/c_1$ interface. (**c**) The water-binding site within the c_1 subunit. (**d**) The Na^+-binding site at the $c_1/c_{2/3}$ interface. Dashed lines indicate inferred hydrogen-bonds in (a) and (c), and ion-protein contacts in (b) and (d). (**e**) F_o-F_c difference map (green mesh) for all bound Na^+ and water molecules, contoured at +5.0σ. The ring is viewed from the cytoplasmic side. (**f**) F_o-F_c maps for either Na^+ or water molecules (yellow and green mesh, respectively) bound within c_1 and the $c_1/c_{2/3}$ interface, contoured at +4.0σ. The $2F_o-F_c$ map for the protein is also shown, contoured at 2.4σ (light blue mesh). Supplementary Fig. 6 shows a stereo-view of this figure.

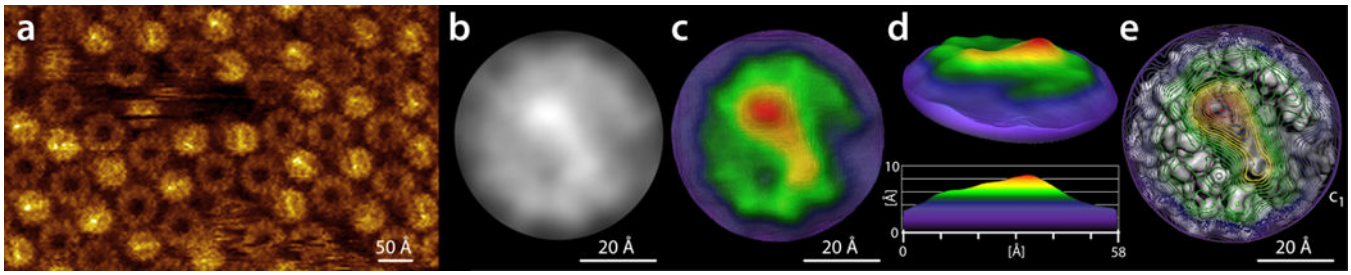

Figure 3.

High-resolution AFM of the *A. woodii* c-ring. (**a**) Topograph of *A. woodii* c-rings densely reconstituted in a lipid membrane[22], with kind permission from the publisher). (**b**) Representative class-average of the periplasmic face of the c-ring, from single-particle analysis (see also Supplementary Fig. 7). (**c**) Density data calculated from (b), colored according to height. (**d**) Same data as in (c), viewed diagonally and in cross-section. (**e**) Same data as in (c) contoured and overlaid on the molecular surface of the c-ring. The position of subunit c_1 is indicated.

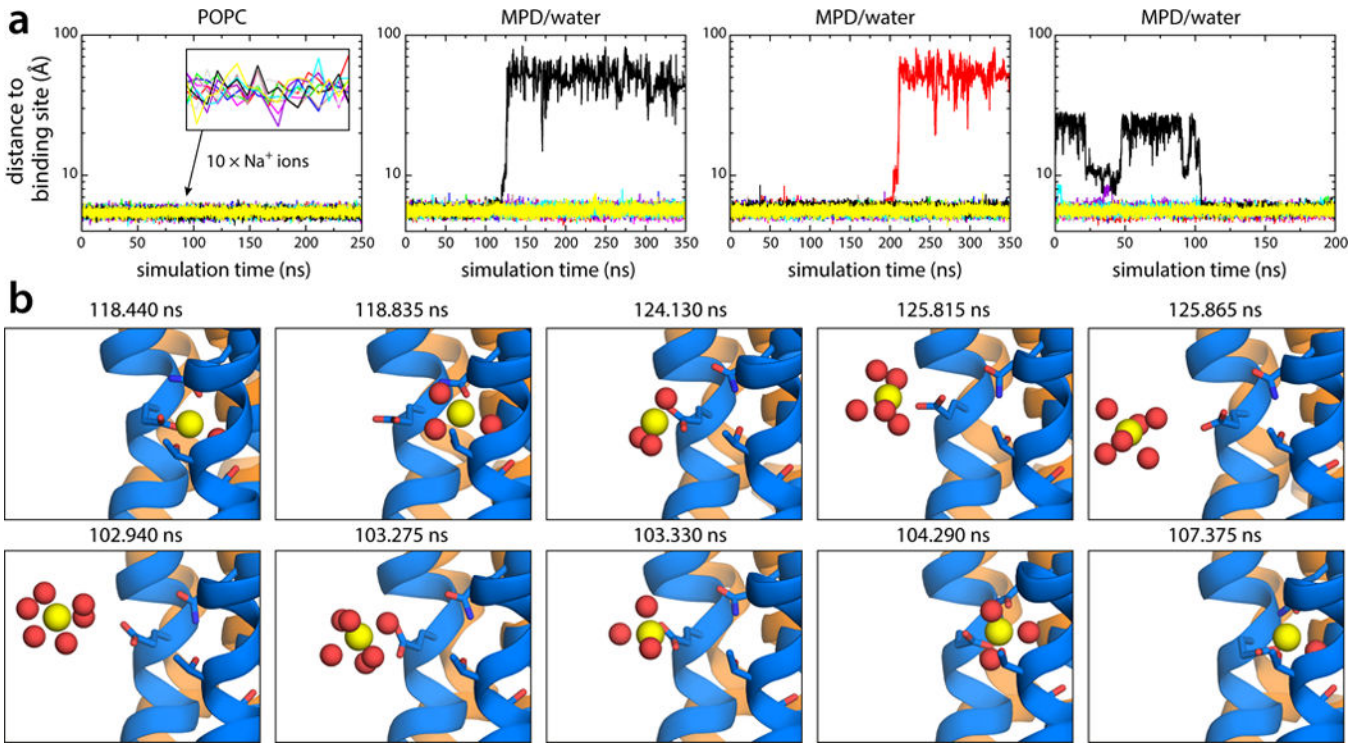

Figure 4.

Spontaneous unbinding and rebinding of Na^+ from/to the *A. woodii* c-ring in molecular dynamics simulations. (**a**) Time-series of the distance between each of the ten Na^+ ions bound to the *A. woodii* c-ring and the neighboring inner helix (residue Pro25 in $c_{2/3}$ subunits, or Pro42 in c_1), in three independent simulations in which the ring is either embedded in a phospholipid membrane (Supplementary Fig. 8), or solubilized in 30% MPD/water (Supplementary Figs. 8, 9) (two simulations), representing the two different micro-environments of the ion-binding sites as the c-ring rotates against subunit-a. The time-trace for each ion is colored differently. (**b**) Representative simulation snapshots during the unbinding (upper panels) and rebinding reactions (lower panels) reveal the atomic mechanism of Na^+ recognition and release. The time-stamp for each snapshot is indicated. Note that the configuration of the unbound site prior to Na^+ rebinding is uncorrelated from that immediately after Na^+ release (Supplementary Fig. 9). The c-ring is colored as in Fig. 1. Side-chains and water molecules (sticks and red spheres, respectively) coordinating Na^+ (yellow spheres) are highlighted. Hydrogen atoms, other protein side-chains and buffer molecules are omitted for clarity.

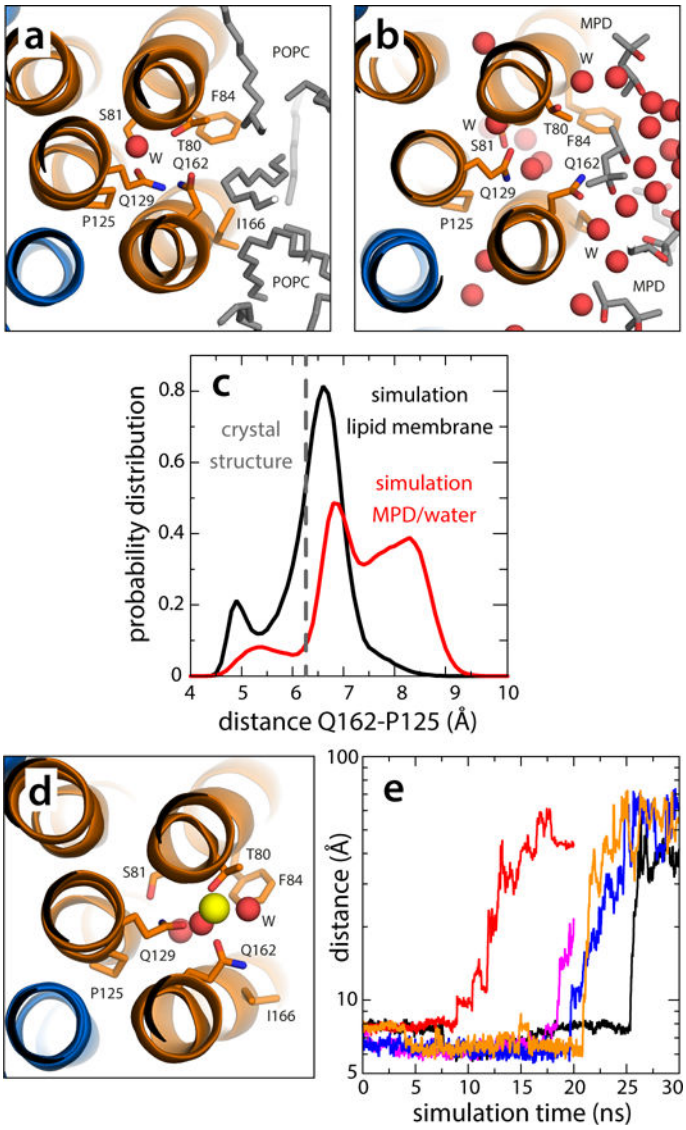

Figure 5.

Dynamics of the vacant site in the V-type c_1 subunit. (**a**) Close-up of the c_1 site, viewed from the cytoplasm, in a representative snapshot of the simulation of the c-ring in a phospholipid membrane (Supplementary Fig. 7). The configuration closely resembles the locked conformation observed in the crystal structure of the c-ring in detergent. (**b**) Close-up of the c_1 site in a representative snapshot of the simulation of the c-ring in the MPD/water buffer (Supplementary Figs. 7, 8). Polar interactions with the buffer unlock the H-bonding interaction network within the site, allowing Gln162 to project away into the solvent. The c-ring is represented as in Fig. 1. Side-chains and water molecules in the site, as well as neighboring lipid tails or MPD molecules, are highlighted (sticks, spheres). Hydrogen atoms as well as other protein side-chains and lipid head-groups are omitted for clarity. (**c**) Probability distributions of the distance between the carboxamide group of Gln162 and Pro125, in the neighboring inner helix, in either simulation, demonstrate the propensity of the c_1 site to adopt an open conformation in the hydrated environment. (**d**) Hypothetical

configuration of the c_1 site with a bound Na^+, equilibrated through restrained molecular dynamics simulations. Note the ion is penta-coordinated, as in the actual Na^+-binding sites. (**e**) Rapid, spontaneous dissociation of the Na^+ ion modeled in the c_1 site in 5 independent simulation trajectories.

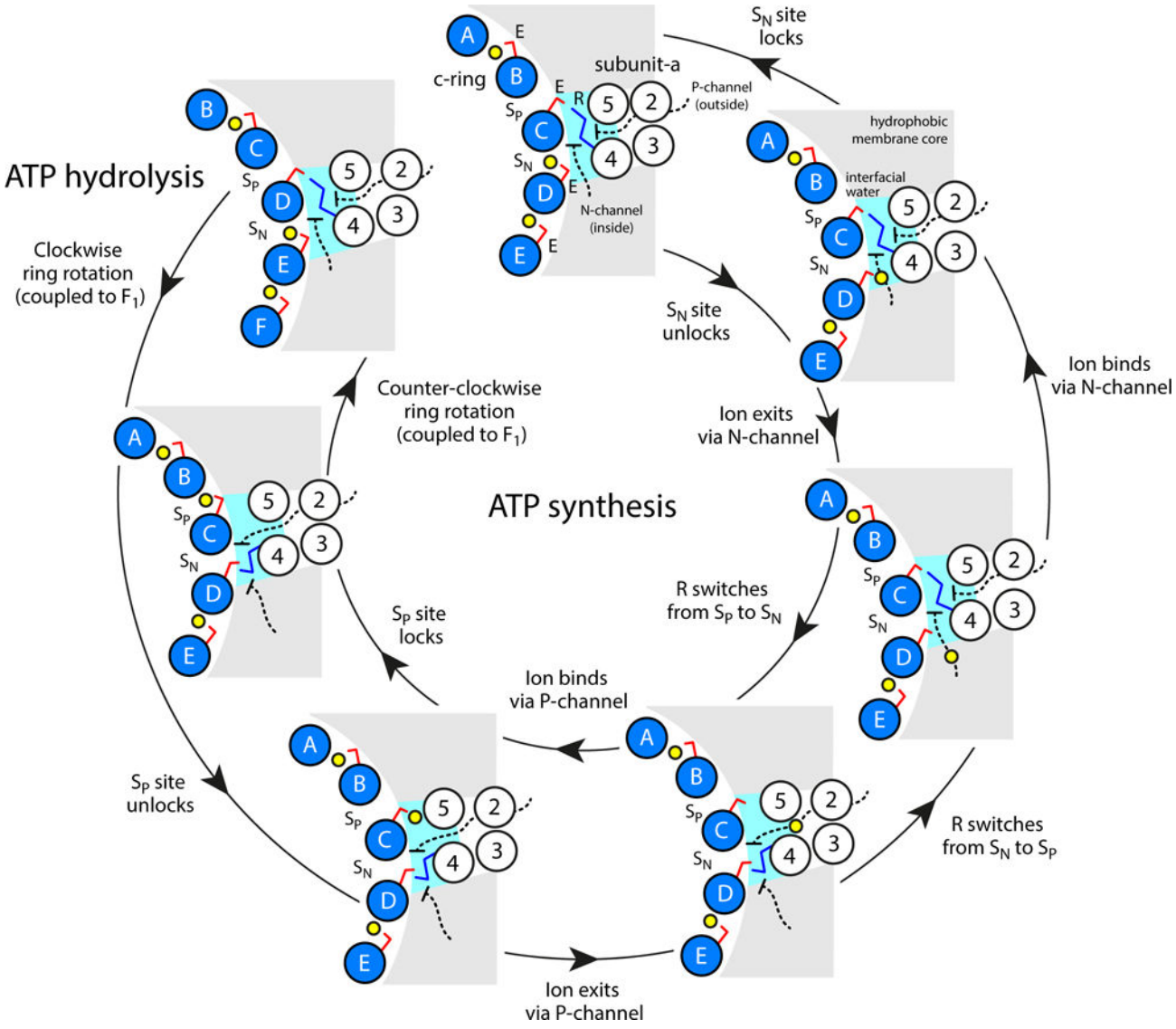

Figure 6.

Proposed microscopic mechanism of c-ring rotation coupled to ion transport. The diagram shows the interface between the c-ring, represented by five of the outer helices (blue circles), and subunit-a, in the topology of TM2-TM5 (white circles) predicted by cross-linking data[64]. Two aqueous half-channels mediate ion exchange across the a/c complex with either the P-side (outside) or the N-side (inside) of the energized membrane (black dashed lines). Hydration of the c-ring binding sites (S_P and S_N, respectively) facilitates loading and release of ions (yellow spheres) via isomerization of a conserved glutamate/aspartate (E, red sticks). A conserved arginine in subunit-a (R, blue sticks) forms alternating salt-bridges with S_P and S_N and thus prevents the ion from hopping between these sites, i.e. it effectively provides an electrostatic barrier between the P and N-channels. The directionality of the mechanism is thus imposed by the clockwise arrangement of S_P and S_N sites: downhill ion permeation (i.e. from P to N) necessarily implies counter-clockwise c-

ring rotations (powering ATP synthesis), while clockwise rotations (driven by ATP hydrolysis) imply uphill transport (i.e. from N to P).

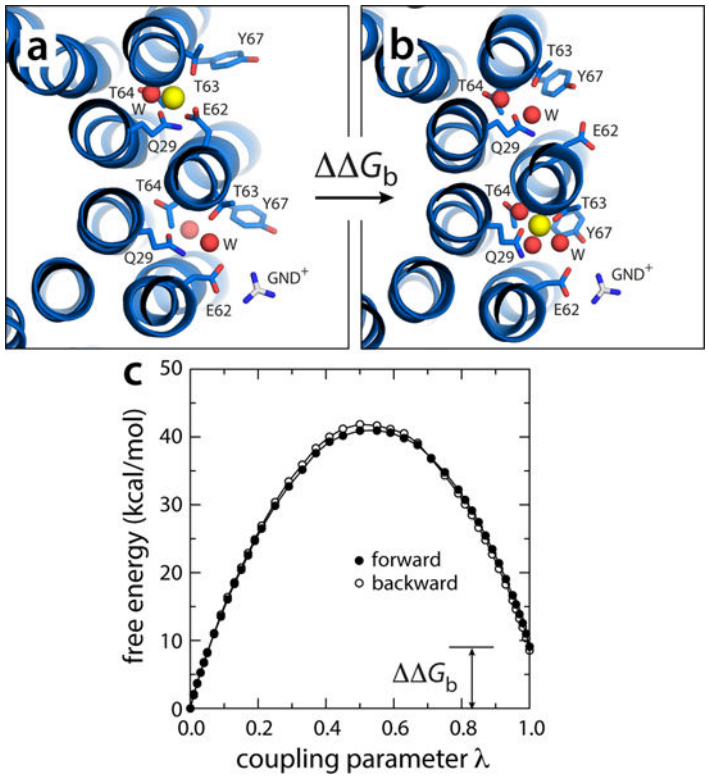

Figure 7.

Electrostatic barrier between the P and N-channels. **(a)** A snapshot was extracted from one of the simulations in which Na^+ is spontaneously released (Fig. 5), and the exposed glutamate side-chain was paired to a guanidinium ion (GND^+), modeled in to represent the interaction with the key arginine side-chain on TM4 of subunit-a. (**b**) The free-energy cost of transferring a bound Na^+ from the adjacent site, counter-clockwise, to the site engaged to the GND^+ ion, was then computed, by gradually decoupling the ion from its environment in configuration (a) and re-coupling it in configuration (b). (**c**) Free-energy change as a function of the (de)coupling parameter λ. The transfer free energy was calculated in both directions. The c-ring is represented as in Fig. 1. Side-chains and water molecules in the site are highlighted (sticks, spheres). Hydrogen atoms as well as other protein side-chains and all MPD/water molecules are omitted for clarity.

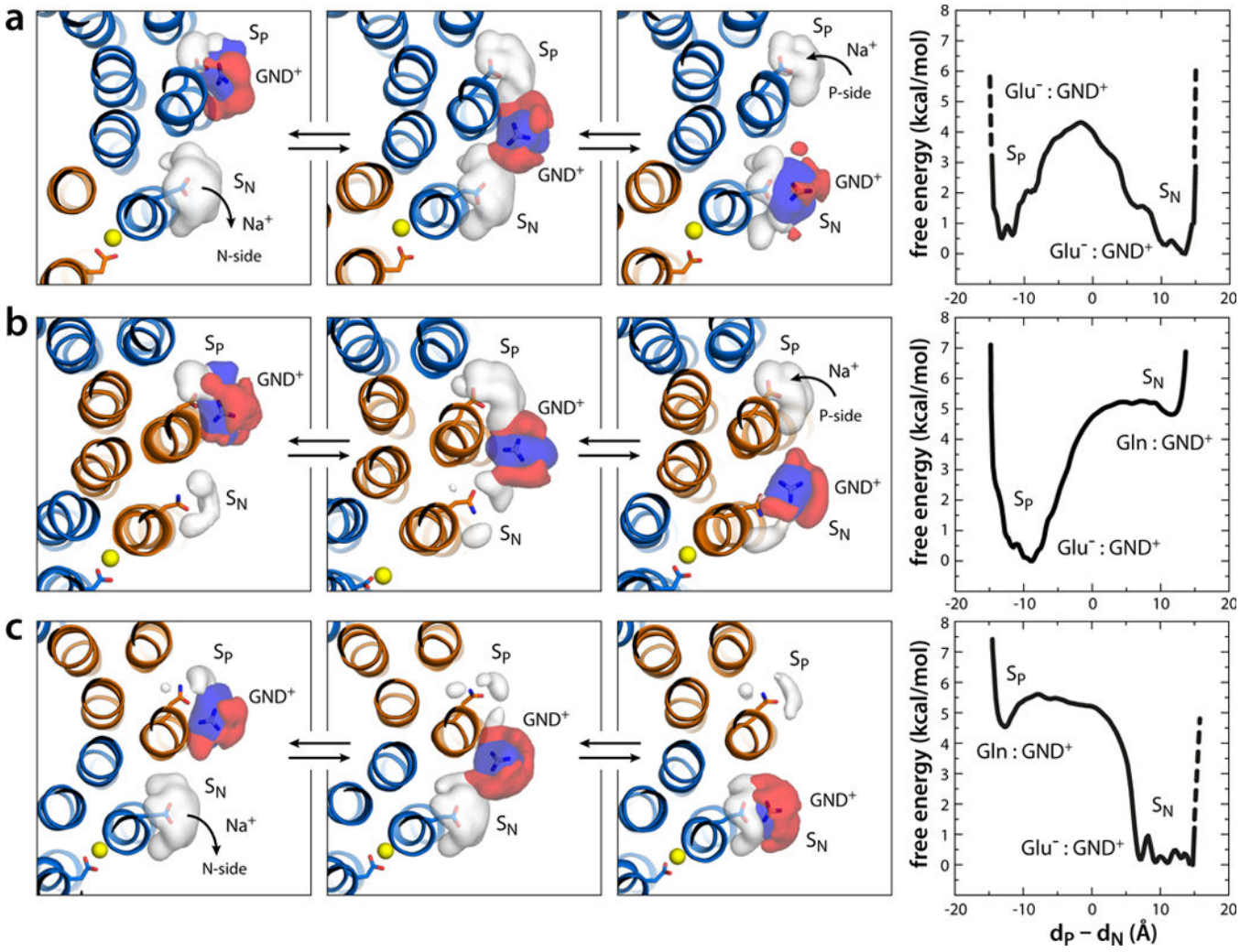

Figure 8.

Energetics of exchange of sequential subunit-a/subunit-c interactions in the rotary cycle. The interaction of the c-subunits with the key arginine on subunit-a was again mimicked with a GND^+ ion (gray/blue sticks) added to the MPD/water buffer. (**a**) GND^+ exchange between two unlocked glutamate side-chains (blue sticks) in adjacent Na^+-binding sites, i.e. after Na^+ release from the S_N site and prior to Na^+ loading to the S_P site. The three panels on the left depict the end-point states in the exchange, and the transition state in between. The colored volumes are density maps extracted from the simulations, mapping the location of either GND^+ (blue), the first hydration shell of GND^+ (red), or the first hydration shell of the carboxylate groups (white). Representative snapshots are shown in Supplementary Fig. 11. The panel on the right shows the free-energy profile associated with the exchange, as a function of the distances between the GND^+ ion and S_P and S_N (d_P and d_N). A two-dimensional free-energy surface is shown in Supplementary Fig. 11. (**b**) Exchange between the unlocked glutamine side-chain in the c_1 subunit (orange sticks) and the glutamate side-chain in the adjacent Na^+ site, counter-clockwise. (**c**) Same as (b), clockwise. The c-ring is represented as in Fig. 2. Hydrogen atoms as well as protein side-chains and MPD/water molecules are omitted for clarity.

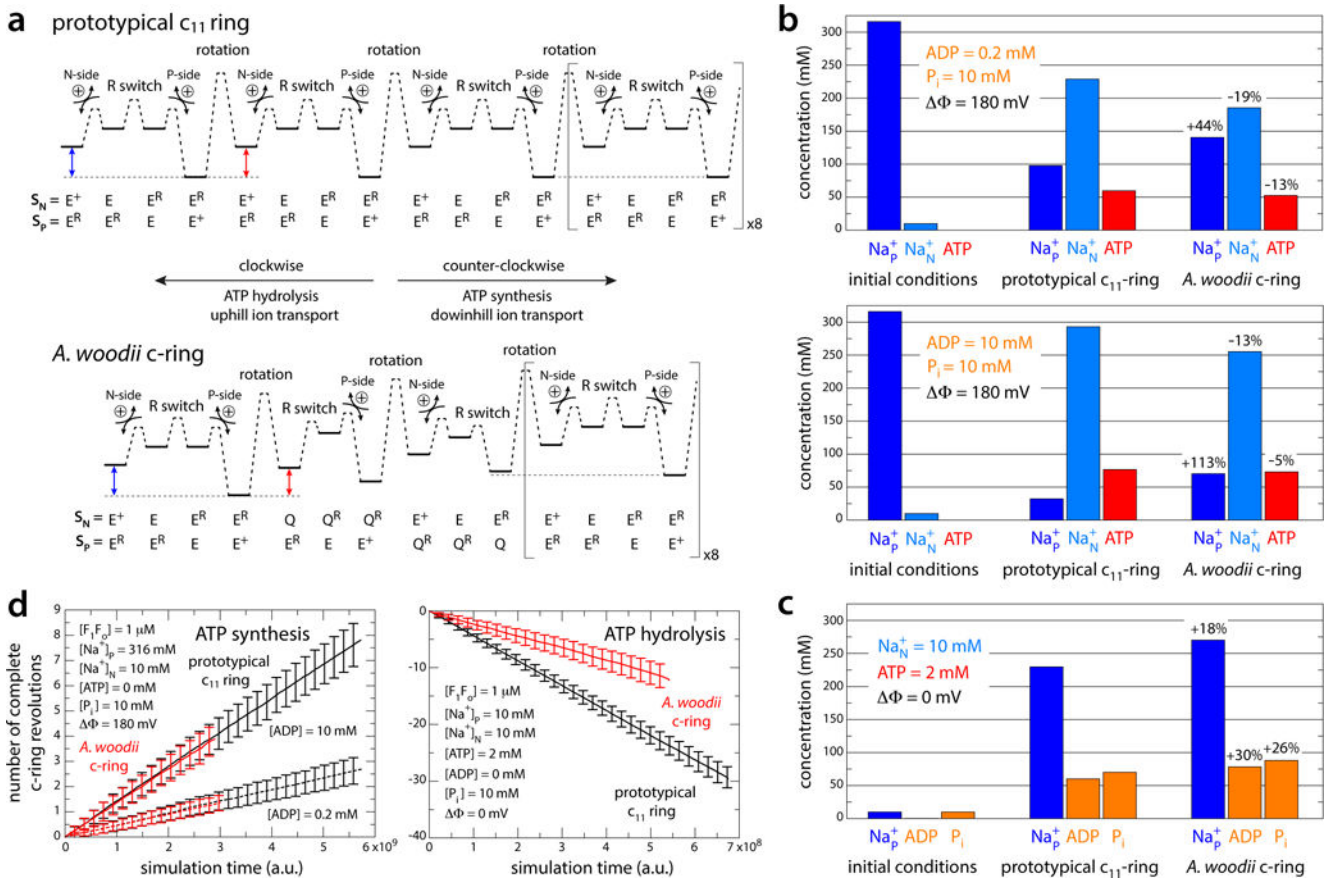

Figure 9.

Thermodynamic impact of the c_1 subunit on ATP synthesis and ion transport. **(a)** Hypothetical free-energy profiles of the c-ring/subunit-a complex, coupled to F_1, for a prototypical F-type c_{11}-ring with no missing ion-binding sites, and for the *A. woodii* c-ring. The profiles illustrate the microscopic states, free-energy differences and kinetic barriers employed in the kinetic model of the rotational cycle described in the text. These states are individually identified by the configuration of the S_P and S_N sites, i.e. whether they feature a glutamate (E) or glutamine (Q), whether they are occupied by Na^+ (E^+) or not (E, Q), and whether they are paired with the arginine on subunit-a (E^R, Q^R) (Methods). The profiles shown represent an equilibrium condition in which the sodium-motive force (blue arrow) and the phosphorylation potential (red arrow) are exactly balanced. The simulations are, however, initiated out of equilibrium, i.e. the landscapes are heavily tilted in one or other direction, favoring ion-driven ATP synthesis or ATP-driven uphill transport, reaching equilibrium gradually. **(b)** Production of ATP driven by a variable transmembrane Na^+ gradient (30-fold initially), under a constant membrane potential of 180 mV i.e. mimicking a voltage-clamp electrophysiological experiment in which the potential is set with K^+ and valinomycin. The values of [ATP], $[Na^+]_P$ and $[Na^+]_N$ at equilibrium are compared with those set initially; percentage differences between the values calculated for an ATP synthase with a prototypical c_{11} ring and the *A. woodii* enzyme are indicated. (**c**) Generation of a transmembrane Na^+ gradient, under a constant membrane potential of 0 mV, driven by an excess of ATP over ADP and P_i. Equilibrium values for a prototypical c_{11} ring and that in *A.*

woodii are again compared. (**d**) Initial rotation rates under the same conditions used in (b) and (c). The data are averages over 100 independent kinetic Monte-Carlo trajectories of 20 million steps each (Supplementary Fig. 13).